이학박사학위논문

Analysis of Gravity Measurements to Understand the Structure and Evolution of the Ulleung Basin (East Sea/Sea of Japan) and Numerical Modeling on the Genesis of Adakites in Subduction Zones

울릉 분지의 성인과 구조에 대한 중력 자료의 분석과 섭입대에서의 아다카이트 생성에 관한 수치 모델링 연구

2016년 2월

서울대학교 대학원

지구환경과학부

김 윤 미

Analysis of Gravity Measurements to Understand the Structure and Evolution of the Ulleung Basin (East Sea/Sea of Japan) and Numerical Modeling on the Genesis of Adakites in Subduction Zones

Yoon-Mi Kim

A dissertation submitted to Graduate School of Seoul National University in partial fulfillment of the requirements for the degree of Doctor of Philosophy

School of Earth and Environmental Sciences
Seoul National University

February 2016

Contents

Chapter 2 Analysis of marine gravity anomalies in the Ulleung Basin (East Sea/Sea of Japan) and its implications for the architecture of rift-dominated backarc basin

Abstract

This thesis presents the results of my studies concerning the tectonic evolution of the Ulleung Basin, East Sea using geological and geophysical data and the genesis of adakites and boninites by partial melting of oceanic crust in subduction zones. My thesis comprises two chapters and first is about the effect of time-varying subduction parameters on the Cenezoic adakites and boninites and next is the analysis of gravity measurements in the Ulleung Basin and its implications for the Moho depth variations.

Chapter 1 addresses the effect of time-evolving slab age and convergence rate of the incoming oceanic plate on the genesis of adakites and boninites in the subduction zones. I made a series of two-dimensional numerical models using the time-dependent subduction parameters and compared with the geochemical evidence in each subduction zones. The results show that my model calculations successfully explained the adakites and boninites in some subduction zones. However, in the other regions such as Mariana and northeastern Japan subduction zones, the other tectonic settings of back-arc spreading, inflow of hot mantle and ridge subduction are needed to explain the partial melting of oceanic crust in subduction zones.

Chapter 2 includes the analysis of gravity measurements in the Ulleung Basin and its implications for the crustal structure. I examined the gravity anomaly of the Ulleung Basin using more extensive data sets focusing on the crustal thickness and also calculated the effect of temperature on the gravity anomaly using a simple thermal model. My analysis shows that the Moho discontinuity is varied from 16 to 22 km, but within the central part of the basin, the variation is only about 10-20 %. Such finding appears to be consistent with previous studies using ocean bottom seismometers. Based on the gravity analysis, I provide the information of crustal structure and infer the

important tectonic processes shaped the Ulleung Basin during post-rift period.

List of Figures

Chapter 1

motion is shown by the black arrow. (b–c) Time-evolving age and convergence rate of the subducting plate in the Izu–Bonin and Mariana subduction zones. Yellow shading denotes the possible period of slab melting from our model calculations, and diagonal-line shading indicates the age of adakites or boninites from geochemical observations. (d–e) Depth versus calculated temperature curves from our model calculations. Solid lines correspond to slab surface temperature at every 10 Myr, and the red dotted line represents the temperature from the steady-state model. The black dashed lines represent the low (triangle) and high (square) end-members of wet basalt and the solidus of wet pelagic sediments (circle), respectively.

Figure 1.4 Temperature and velocity in the Mariana subduction zone at 45, 40, 35, 30, 25, and 20 Ma. The unit of temperature is degree Celsius (°C), and the contour is drawn at every 100°C. The arrows in the mantle wedge indicate mantle flow velocity. The flows in the mantle wedge are dynamically calculated, and the top and bottom boundaries of the mantle wedge are shown with dashed red lines. The blue arrows denote the convergence rate of the subducting slab.

Figure 1.5 (a) Schematic map of the northeast Japan and Kuril subduction zones with major plate boundaries (black lines). (b–c) Time-evolving slab age and convergence rate of the subducting plate in the northeast Japan and Kuril subduction zones. (d–e) Depth versus calculated temperature curves from our model calculations. All shadings, lines, and arrows are the same as in Fig. 1.3.

Figure 1.6 (a) Schematic map of the Tonga subduction zone with major plate

boundaries (black lines). The black star and circle indicate the locations of the North Tonga adakites/boninites and the boninites from the central portion of the Tonga forearc, respectively. (b) Time-evolving age and convergence rate of the subducting plate at Tonga. (c) Depth versus calculated temperature curves from our model calculations. All shadings, lines, and arrows are the same as in Fig. 1.3.

Figure 1.7 (a) Schematic map of the Java–Sunda subduction zone with major plate boundaries (black lines). (b–c) Time-evolving slab age and convergence rate of the subducting plate in the northwestern and southeastern Java–Sunda. (d–e) Depth versus calculated temperature curves from our model. All shadings, lines, and arrows are the same as in Fig. 1.3.

Figure 1.8 (a) Schematic map of the Aleutian subduction zone with major plate boundaries (black lines). (b–c) Time-evolving slab age and convergence rate of the subducting plate in the western and eastern Aleutians. (d–e) Depth versus calculated temperature curves from our model calculations. All shadings, lines, and arrows are the same as in Fig. 1.3.

Figure 1.9 Profiles of surface slab temperature at a 90-km depth in our model calculations. The blue and red lines denote slab surface temperatures from the time-dependent and steady-state subduction models, respectively. Yellow shading represents temperature higher than the wet basalt solidus of Schmidt and Poli (1998) at a depth of 90 km, which is a possible region for partial melting of oceanic crust.

Chapter 2

Figure 2.1 (a) Physiographic map of the East Sea/Sea of Japan. Dotted box locates the study area. JB, YB and UB: Japan, Yamato and Ulleung basins, KP: Korea Plateau, YR: Yamato Ridge, OB: Oki Bank. (b) Bathymetric map of the Ulleung Basin and contour interval is 500 m. UI: Ulleung Island, AS: Anyongbok Seamount, DI: Dok Island, SS: Simheungtaek Seamount

Figure 2.2 (a) Color shaded-relief free-air gravity anomaly map superimposed onto bathymetry. The free-air gravity was measured by R/V Tamhae II from 1997 to 2014. Contour lines of bathymetry are at 500 m depth interval. The red dotted lines locate the gravity comparison in (b). (b) Comparison between shipboard gravity data (black) and satellite-derived gravity data (red). The satellite gravity data is derived from satellite altimeters (Sandwell and Smith, 1997).

Figure 2.3 Free-air gravity anomaly map derived from the satellite altimeters. Contour interval is 20 mGal and abbreviations are same in Fig. 2.1.

Figure 2.4 Basement topography map. Contour interval is 1000 m and gray shading at right corner denotes the region where the data of sediment thickness is not available. The white dotted line encloses the region of basement median high and abbreviations are same in Fig. 2.1.

Figure 2.5 Residual gravity anomaly (RGA) map eliminated the gravitational effect of the seafloor and sedimentary basement from the free-air anomaly. Contour interval is 20 mGal. Abbreviations are same in Fig. 2.1 and gray shading is the same as shown in Fig. 2.4.

Figure 2.6 (a) Shaded-relief map of the Moho discontinuity derived from residual gravity anomaly (RGA). Color shaded is the area where the data of sediment thickness is reliable in the Ulleung Basin. The contour interval is 1 km. 'H' indicates the region showing the highest Moho topography and the black dashed line is the extrapolation of high-value of the Moho depth. The red dotted lines denote the location of cross sections in (b). Red triangles is volcanic edifices erupted during the Quaternary period and blue triangle indicates the location of intrusive magmatic body. Abbreviations are same in Fig. 2.1 and gray shading is the same as shown in Fig. 2.4. (b) Cross sectional views showing the boundaries of the water, sediment, crust and mantle across the A-A', B-B', C-C' and D-D' lines in (a).

Figure 2.7 Schematic diagrams indicating the thermal model for the Ulleung Basin assuming mantle potential temperature of 1300 °C and stretching factor of 3 (Crustal and lithospheric thickness decrease from 30 to 10 and 100 to 33 km, respectively.). The half-space cooling model was used to calculate the geotherms and pure shear opening of McKenzie (1978) is applied. (a) At time = 0 Myr, extension of the basin occurs instantaneously and causes upwelling of the asthenosphere. The lithosphere cools down by thermal conduction and thickens with age. The temperature of base of the lithosphere is assumed as 1000°C (Leeds et al., 1974). (b) At time = 25 Myr after instantaneous thinning by lateral stretching for β=3, the thickness of lithosphere goes down at about 55 km by thermally conductive cooling. The units of density (ρ) and thermal conductivity (k) are g/cm^3 and W/m/K, respectively.

Figure 2.8 Variation of gravity anomaly by conductive cooling during 25 Myr after instantaneous thinning. The stretching factor (β) for 2 and 3 and the

potential temperature (Tm) for 1300 and 1400°C were used in our model (described in Fig. 2.7). (a) Fixed that stretching factor (β) is 3, comparison of gravity anomaly variation calculated using the mantle potential temperature (Tm) for 1300 and 1400°C. (b) Fixed that mantle potential temperature (Tm) is 1400°C, comparison of gravity anomaly variation calculated using the stretching factor (β) for 2 and 3. Double-headed arrow denotes the amount of the variation of the residual gravity anomaly (RGA) which is about 80 mGal in the Ulleung Basin (Fig. 2.5).

Figure 2.9 Simple diagram showing the gravity anomaly caused by intrusive volcano. (a) Gravity anomaly caused by 2.4 (dashed), 2.5 (dotted) and 2.6 g/cm^3 (solid) of intrusive volcano within the sediment described as red triangle in (b). (b) Profile of intrusive magmatic body including density values of water (1.0 g/cm^3) and sediment (2.3 g/cm^3). The width and height of the intrusive volcano are modified from Kim et al. (submitted) and its location is described in Fig. 2.6 (blue triangle).

Figure 2.10 Model diagram illustrating the flexural bulge by sediment loading to the south and magmatic underplaing by volcanic edifices to the north of the Ulleung Basin.

List of Table

Chapter 1

Chapter 1

Effect of time-evolving age and convergence rate of the subducting plate on the Cenozoic adakites and boninites

Abstract

Partial melting of subducting oceanic crust expressed as high-Mg volcanic rocks such as adakites and boninites has been actively studied for decades, and Lee and King (2010) reported that time-evolving subduction parameters such as the age and the subduction rate of the converging oceanic plate play important roles in transient partial melting of the subducting oceanic crust (e.g., Aleutians). However, few subduction model experiments have considered time-evolving subduction parameters, posing problems for studies of transient partial melting of subducting oceanic crust in many subduction zones. Therefore, we constructed two-dimensional kinematic-dynamic subduction models for the Izu–Bonin, Mariana, northeast Japan, Kuril, Tonga, Java–Sunda, and Aleutian subduction zones that account for the last 50 Myr of their evolution. The models include the time-evolving age and convergence rate of the incoming oceanic plate, so the effect of time-evolving subduction parameters on transient partial melting of oceanic crust can be evaluated. Our model calculations revealed that adakites and boninites in the Izu–Bonin and Aleutian subduction zones resulted from transient partial melting of oceanic crust. However, the steady-state subduction model using current subduction parameters did not produce any partial melting of oceanic crust in the aforementioned subduction zones, indicating that time-evolving subduction parameters are crucial for modeling transient eruption of adakites and boninites. Our model calculations confirm that other geological processes such as

forearc extension, back-arc opening, mantle plumes and ridge subduction are required for partial melting of the oceanic crust in the Mariana, northeast Japan, Tonga, and southeastern Java–Sunda subduction zones.

Keywords: adakite, arc volcano, numerical modeling, subduction zone

1.1. Introduction

Arc magmatism in subduction zones is a manifestation of complex physical and chemical processes in the subducting slab, mantle wedge, and overlying crust. Because subduction is a transient process, arc magmatism in subduction zones also exhibits transient behaviors, such as across-arc migration of volcanism and variation in magmatic rock types through space and time (e.g., Kay et al., 2005; Kelemen et al., 2003; Straub and Zellmer, 2012).

Most arc magmatism is thought to result from partial melting of the mantle wedge triggered by the influx/addition of volatiles released from the subducting slab. However, some volcanic rocks are thought to originate from partial melting of the eclogitized oceanic crust of the subducting slab (Defant and Drummond, 1990; Kay, 1978). Typical examples include the well-known adakites in the Aleutians (Defant and Drummond, 1990; Kay, 1978; Stern and Kilian, 1996), bajaites in Baja California (Rogers et al., 1985; Saunders et al., 1987), and sanukitoids in southwest Japan (Koto, 1916; Stern et al., 1989; Tatsumi and Ishizaka, 1981), named after the region where the rocks were discovered. For convenience, we hereafter call the rock ‘adakite’ if it originated from partial melting of subducting oceanic crust. Additionally, the boninites in the Bonin Islands (Cameron et al., 1979; Kuroda et al., 1978) are thought to be attributable to mixing between partial melts from the mantle wedge and eclogitized oceanic crust. Because a cold subducting slab is unlikely to undergo partial melting, unusual tectonic environments such as subduction zones with a very young subducting slab (<25 Ma), ridge subduction, or flat subduction are generally proposed as sites of adakite genesis (Defant and Drummond, 1990; Gutscher et al., 2000; Kay, 1978; Maruyama et al., 1996; Peacock, 1996). Additionally, recent studies have indicated that

plume-slab interaction, cold plumes, and the injection of hot asthenospheric mantle into the corner of the mantle wedge are responsible for the partial melting of oceanic crust (Gerya and Yuen, 2003; Kincaid et al., 2013; Lee and Ryu, accepted; Yamamoto and Hoang, 2009).

Recent studies have shown that some 'adakite-like' rocks are geochemically similar to adakites but are not produced by the partial melting of subducting oceanic crust (e.g., Chung et al., 2003; Gerya and Yuen, 2003; Guan et al., 2012; Kay and Kay, 1993; Lai and Qin, 2013; Richards and Kerrich, 2007). These studies suggested that such adakite-like rocks could be generated in a variety of tectonic environments: partial melting of relaminated oceanic plate in the mantle wedge, crystal fractionation of basaltic magma, and partial melting of thickened mafic lower crust or delaminated lower crust in the intracontinental region. Castillo (2012) distinguished between adakites and adakitic rocks: adakites are characterized by lower $^{143}Nd/^{144}Nd$ ratios and higher $^{87}Sr/^{86}Sr$ compared with adakite-like rocks. Hereafter we use the term 'adakitic rock' if the rock originated from processes other than partial melting of subducting oceanic crust but has geochemistry similar to that of adakite.

Adakites and boninites have been recovered in the Izu–Bonin–Mariana, northeast Japan, and Tonga subduction zones, where partial melting of subducting oceanic crust is not expected from the current slab age and convergence rate (e.g., Defant and Drummond, 1990; Gutscher et al., 2000; Peacock, 1996). Therefore, other mechanisms for partial melting of oceanic crust have been suggested to explain these adakites or boninites. In the Izu–Bonin–Mariana subduction zone, previous studies have suggested that Early Eocene boninites were generated by forearc extension during the subduction initiation or by a hot mantle plume (Pearce et al., 1992; Stern and

Bloomer, 1992). The adakites in northeast Japan were generated by the effect of the back-arc opening of the East (Japan) Sea (Yamamoto and Hoang, 2009), and the origin of Tonga boninites is deeply related to back-arc spreading in the Lau Basin (Cooper et al., 2010).

However, the mechanisms described above are only possible explanations for the existence of adakites or boninites. Additionally, the time-evolving slab age and convergence rate constrained from plate reconstruction models, which were not incorporated in previous studies, may play crucial roles in the genesis of adakites or boninites. For example, numerical modeling experiments by Lee and King (2010) revealed that the time-evolving age and convergence rate of the subducting plate are responsible for localized occurrences of adakites in the western Aleutians. Plate reconstruction models (Sdrolias and Müller, 2006) have revealed that convergence rate and slab age have changed greatly over time even in the same subduction zone, which suggested that past arc volcanism is a consequence of past subduction environments, affected by past slab age and convergence rate rather than current slab age and convergence rate. Thus, time-evolving numerical model experiments are necessary to clarify arc magmatism. Despite the importance of these subduction parameters, many steady-state numerical model experiments use the constant slab age and convergence rate to infer the past arc magmatism (e.g., Baitsch-Ghirardello et al., 2014; Peacock, 1996; Syracuse and Abers, 2006; van Keken et al., 2002).

In our study, we formulated a series of two-dimensional numerical model experiments including time-evolving age and convergence rate of the subducting oceanic plate that are constrained by recent plate reconstruction models (Sdrolias and Müller, 2006) to investigate the transient partial melting of the oceanic crust in the Izu–

Bonin, Mariana, northeast Japan, Kuril, Tonga, Java–Sunda, and Aleutian subduction zones (Fig. 1.1). Other subduction zones, such as the Cascadia, southwest Japan, and southern Chile are not considered in this study because a very young subducting slab, ridge subduction and/or flat subduction are the likely causes of the partial melting of oceanic crust in the subduction zones. The next sections compare these model calculations with the results of geochemical and petrological studies, and discuss possible reasons for inconsistencies.

1.2. Numerical model

To examine the partial melting of oceanic crust, a series of two-dimensional time-dependent subduction models were formulated for the Izu–Bonin, Mariana, northeast Japan, Kuril, Tonga, Java–Sunda and Aleutian subduction zones. Because most of the numerical experiments conducted in this study are based on previous studies (Lee and King, 2009, 2010), the scheme and rheology used in the experiments are introduced only briefly here. Time-evolving slab age and convergence rate were obtained from the plate reconstruction model of Sdrolias and Müller (2006) at interval of every 5 Ma and were interpolated using piecewise polynomials to approximate the evolving slab age and convergence rate. Although slab dip changes with depth (Syracuse and Abers, 2006), we used a constant dip of 30, 45, or 60 degrees from the depths of 50–200 km: 30° for the northeast Japan, 45° for the Izu–Bonin, Kuril, Tonga, Java–Sunda, and eastern Aleutians, and 60° for the Mariana and western Aleutians (Fig. 1.2). Although some studies have reported that slab dip changes with time due to slab buckling and trench migration (advance or retreat) (Funiciello et al., 2003; Lee and King, 2011), we did not consider variation in slab dip and trench migration to avoid

numerical difficulties and costs. The slab age and convergence rate of the subducting slab was kinematically prescribed using the interpolated slab age and convergence rate, and a 35-km-thick overriding plate was assumed during the entire runs of the subduction experiments. Mantle behavior in the mantle wedge was assumed to be dominated by corner flow driven by the subducting slab and mantle buoyancy in the mantle wedge was neglected.

The rheology of the mantle wedge was expressed as a composite viscosity of diffusion and dislocation creep as described in Lee and King (2009, 2010). Rheological parameters for the diffusion and dislocation creep were based on Karato and Wu (1993). Because the mantle wedge is hydrated by water released from the upper part of the subducting slab, we reduced the mantle viscosity at the corner of the mantle wedge to 1/20 the calculated composite viscosity of diffusion and dislocation creep (Honda and Saito, 2003; Lee and King, 2010). Previous studies have reported that the corner of the mantle wedge is considerably serpentinized by hydration (Brocher et al., 2003), and the serpentinized corner may not be involved in corner flow due to the lower density of the serpentinite. Therefore, the corner of the mantle wedge was isolated by extending the overriding lithosphere to depth of 50 km.

The depth of the model domain is 200 km, and the width of the model domain is varied with slab dip: 350 km for Izu–Bonin, Kuril, and Tonga (slab dip: 45°); 509 km for northeast Japan (slab dip: 30°); 271 km for Mariana and western Aleutians (slab dip: 60°); and 400 km for Java–Sunda and eastern Aleutians (slab dip: 45°) (Fig. 1.2). All model domains consist of four-node quadrilateral elements of which height is maintained at 1 km but width is varied according to slab dip. The half-space cooling model (Stein and Stein, 1992) was used to calculate the thermal structure of the

incoming plate for a given age, and mantle potential temperature was assumed to be 1450°C, the upper limit of reported mantle temperature (Asimow et al., 2001; Putirka et al., 2007). The finite element code based on the incompressible Boussinesq approximation (ConMan; King et al., 1990) was used to calculate the kinematic and dynamic behavior of the mantle and subducting slab. Time-evolving slab age and convergence rate were updated along the left boundaries at each time step for the entire modeling run.

1.3. Results

1.3.1. Izu–Bonin–Mariana (IBM)

Fig. 1.3 presents the time-dependent variations of slab age and convergence rate used in our numerical model calculations (Figs. 1.3b and 1.3c) and the resultant time-dependent evolutions of slab surface temperature (Figs. 1.3d and 1.3e) since 50 Ma calculated for the Izu–Bonin and Mariana subduction zones.

According to our models, in the Izu–Bonin subduction zone (Fig. 1.3d), slab surface temperature was beyond both the solidi of wet sediments (Nichols et al., 1994) and wet basalt (Kessel et al., 2005; Schmidt and Poli, 1998) from ca. 50–25 Ma, resulting in partial melting of the overlying sediment and eclogitized oceanic crust. In the Mariana subduction zone, partial melting is expected to have occurred from ca. 40–30 Ma (Fig. 1.3e).

Fig. 1.4 presents the temperature and mantle flow velocity in the Mariana

subduction zone at 45, 40, 35, 30, 25 and 20 Ma using a 5 Myr interval. The depiction of mantle flow velocity is limited to the mantle wedge where dynamic calculation was carried out. A high convergence rate of the subducting slab resulted in vigorous corner flow in the mantle and increased the temperature of the corner of the mantle wedge, and vice versa (Figs. 1.4a and 1.4f vs. 1.4b, 1.4c, and 1.4d). Increased slab velocity resulted in a thin thermal boundary layer on the subducting slab (Figs. 1.4a and 1.4f). The mantle temperature at the corner of the mantle wedge decreased until 30 Ma as the convergence rate decreased. From 25 Ma, the convergence rate and temperature in the mantle wedge began to increase with time. The fast and slow mantle flow velocities at the corner of the mantle wedge are strongly correlated with the convergence rate because mantle behavior in the mantle wedge is dominated by slab behavior.

Geochemical studies on the Izu–Bonin and Mariana subduction zones have revealed that boninitic volcanism occurred during the Middle Eocene, indicating partial melting of eclogitized oceanic crust (Ishizuka et al., 2006; Macpherson and Hall, 2001; Pearce et al., 1992). The Eocene boninites in the Izu–Bonin (46–48 Ma from $^{40}Ar/^{39}Ar$ age dating; Pearce et al., 1992) are consistent with the partial melting of oceanic crust in our model calculations (ca. 50–25 Ma), whereas the boninites in the Mariana (45–49 Ma; Hickey-Vargas et al., 1989) are not consistent with the period of boninitic volcanism in our model calculations (ca. 40–30 Ma).

We also calculated slab surface temperature from steady-state model calculations using the current slab age and convergence rate (Figs. 1.3d and 1.3e). The steady-state model calculations generate only the partial melting of the overlying sediments, except for the eclogitized oceanic crust, in contrast to the model calculations using time-evolving subduction parameters. The large differences in slab

surface temperature between the time-evolving and steady-state model calculations indicate that the time-evolving slab age and convergence rate are responsible for the boninitic volcanism in the IBM subduction zone.

1.3.2. Northeast Japan–Kuril

The age of the oceanic plate converging to the trench in the northeast Japan and Kuril subduction zones has increased since the along-strike subduction of the mid-ocean ridge bounding the Izanagi and Pacific plates at ca. 60 Ma (Sdrolias and Müller, 2006). Thus, the slab age in northeast Japan and Kuril in our model calculations has been increasing since 50 Ma due to the aging Pacific plate (Figs. 1.5b and 1.5c). Although there are a few variations, the rate of the converging oceanic plate has also increased gradually since 50 Ma, in contrast to the large variations of plate motion in the IBM subduction zone. In the northeast Japan subduction zone, our model results show that the slab surface temperature was beyond the wet basalt solidi from 50–30 Ma, implying partial melting of the eclogitized oceanic crust (Fig. 1.5d). However, the results do not show partial melting of subducting oceanic crust since 30 Ma, and are not consistent with the Abukuma adakites in northeast Japan at ~16 Ma (Hanyu et al., 2006; Sato, 1994; Tatsumi et al., 1989; Yamamoto and Hoang, 2009).

Fig. 1.5e shows that the slab surface temperature in the Kuril subduction zone has decreased gradually since 50 Ma due to increasing slab age and convergence rate, and fall below the wet basalt solidi at ca. 40 Ma. In the Kuril subduction zone, geochemical and petrological studies have indicated that partial melting of oceanic crust has not occurred since the Cretaceous (e.g., Bailey et al., 1989; Martynov et al.,

2012), and Martynov et al. (2010) demonstrated that oceanic sediments are involved in the magma generation in the northern Kuril island arc. Although no evidence for the partial melting of oceanic crust has been reported, our model calculations indicate partial melting of oceanic crust by Late Eocene, since ridge subduction at ca. 60 Ma (Fig. 1.5e).

We conducted steady-state model calculations using the current slab age and convergence rate in northeast Japan and Kuril. Neither experiment revealed any partial melting of eclogitized oceanic crust, which is consistent with the current arc volcanism in the northeast Japan and Kuril. As observed in the model calculations for the IBM subduction zone, time-evolving subduction for the last 50 Myr suggests partial melting of eclogitized oceanic crust in northeast Japan and Kuril during the Paleocene and Eocene.

1.3.3. Tonga

Using the time-evolving slab age and convergence rate in the northern Tonga (Fig. 1.6b), we calculated slab surface temperatures since the subduction initiation at 45 Ma. As expected from the increasing slab age and convergence rate, slab surface temperatures in the Tonga subduction zone decreased gradually with time. Our model calculations indicate that partial melting of the oceanic crust occurred since 45 Ma, although the partial melting waned with time (Fig. 1.6c).

Petrological studies suggest the presence of two representative boninites and adakites in the Tonga subduction zone (Fig. 1.6a). One is high-Ca boninite (black star)

in the northern Tonga forearc near the north end of the trench where the transition from trench to transform fault occurs (Danyushevsky et al., 1995; Falloon et al., 2008), and the ages of the boninites are estimated at ~0.5–3 Ma and ~15.2 Ma based on $^{40}Ar/^{39}Ar$ age dating (Falloon et al., 2008; Meffre et al., 2012). Adakites (black star) have also been recovered in the same region, and their age is estimated at ~2.5 Ma (Falloon et al., 2008). Other high-Ca boninites (black circle), less than 1 Ma, have been found in the Tonga forearc at ~21°S, ~175°W, east of the Eastern Lau Spreading Center (Cooper et al., 2010).

In the Tonga subduction zone, the ages of the two representative high-Ca boninites and adakites are apparently consistent with the slab melting in our model calculations. However, the high-Ca boninites are thought to have been generated at a shallower depth than that of our model calculations, so other tectonic processes may have been responsible for the boninites. Steady-state model calculations using the current age and convergence rate of the incoming oceanic plate revealed no partial melting of oceanic crust, except for overlying sediments on the plate; other tectonic processes are required to explain the genesis of the adakites and boninites.

1.3.4. Java–Sunda

For the Java–Sunda subduction zone, we calculated slab surface temperature in two representative regions, the northwestern and southeastern Sumatra Islands (Fig. 1.7a), because these regions have experienced considerably different time-evolving ages and convergence rates of the incoming oceanic plate (Figs. 1.7b and 1.7c). The Java–Sunda subduction system has existed since at least the Mesozoic (Heine et al.,

2004), and the different evolutions in slab age and convergence rate between the northwestern and southeastern Java–Sunda were the results of complex tectonic settings, exemplified by the eastward-increasing age of the subducting plate along the Sunda trench and the northward migration of Wharton Ridge subduction. The Wharton Ridge was active from 70–43 Ma, and the extinct Wharton Ridge is currently subducting in the Java–Sunda subduction zone (Heine et al., 2004; Krishna et al., 1995).

Figs. 1.7d and 1.7e present slab surface temperatures since 50 Ma in the northwestern and southeastern Java–Sunda subduction zones. Despite large variations in slab age and convergence rate, relatively small variations of slab surface temperature were generated in both the Java–Sunda subduction zones. In the northwestern Java–Sunda subduction zone, our model results show that all the slab surface temperatures are lower than the solidi of oceanic crust, which indicates no partial melting of oceanic crust and is consistent with geochemical studies of the forearc (Pedersen et al., 2010). However, in the southeastern Java–Sunda subduction zone, our model calculations suggest that partial melting of oceanic crust occurred from ca. 50–20 Ma. Because most observational studies have focused on Neogene and Quaternary arc volcanism and no Paleogene data have been reported (e.g., Gertisser and Keller, 2003), it is not clear whether partial melting of oceanic crust did occur from ca. 50–20 Ma in the Java–Sunda subduction zones. However, Gertisser and Keller (2003) proposed that partial melting of the subducting sediment, excepting subducting oceanic crust, resulted in the Holocene medium- and high-K volcanic rocks in the southeastern Java–Sunda, which is consistent with our model calculations indicating the partial melting of the sediments on top of the oceanic crust (Fig. 1.7e). Isotopic and trace element data have also revealed that the incorporation of the subducted sediment is attributable to

heterogeneity in the southeastern Java–Sunda arc (Handley et al., 2011).

Slab surface temperature from the steady-state model produces no partial melting of oceanic crust in either the northwestern or southeastern Java–Sunda subduction zone (Figs. 1.7d and 1.7e), similar to the time-evolving model calculations and geochemical observations in the northwestern Java–Sunda. However, the results of the steady-state model calculation for the southeastern Java–Sunda differed from those of the time-evolving model, demonstrating the possibility of partial melting of subducting oceanic crust.

1.3.5. Aleutians

Lee and King (2010) evaluated the temporal evolution of thermal structures in the Aleutians from time-evolving slab age and convergence rate. We reproduced the thermal structures of the subduction zones using the same parameters and geometries, except we used a slightly higher mantle potential temperature of 1450°C, instead of the 1400°C used by Lee and King (2010).

For the western Aleutians, our model results indicate that slab surface temperature has been beyond the solidi of wet sediments and basalt since 50 Ma (Fig. 1.8d) and that partial melting of oceanic crust occurs extensively, as observed by Lee and King (2010). Geochemical studies have reported that adakites produced by the partial melting of oceanic crust are abundant throughout the western Aleutians (Kay, 1978; Kelemen et al., 2003; Yogodzinski and Kelemen, 1998), which is well consistent with our model calculations. For the eastern Aleutians, our model calculations indicate

that the slab surface temperatures are slightly higher than the solidi of wet basalt, slightly higher than the temperatures in Lee and King (2010), because of the higher mantle potential temperature of 1450°C. However, the partial melting of the oceanic crust is marginal and much weaker than that in the western Aleutians. Our model calculations are consistent with the broad eruptions and intrusions of basaltic and gabbroic rocks with a paucity of adakites in the eastern Aleutians (Kelemen et al., 2003).

The steady-state model calculations show that higher slab surface temperatures in the western Aleutians than that in the eastern Aleutians, consistent with the localized distribution of adakites in the western Aleutians. However, the time-evolving model calculations demonstrate the effects of time-evolving slab age and convergence rate on the partial melting of the oceanic crust in the western Aleutians.

1.4. Discussion

1.4.1. Implications of time-evolving subduction parameters to thermal structure

We conducted a series of two-dimensional numerical subduction model experiments to evaluate whether the partial melting of subducting oceanic crust inferred from adakites and boninites can be correlated with the time-evolving subduction parameters. Our model calculations revealed that the time-evolving age and convergence rate of the subducting oceanic plates could explain the transient adakites and boninites in the Izu–Bonin and western Aleutians.

To clarify the differences between the time-evolving and steady-state model experiments, we compared the slab surface temperatures measured at a depth of 90 km in both model experiments. This depth is thought to be a representative depth for the partial melting of the subducting slab, resulting in adakitic or boninitic magmas (Mibe et al., 2011) (Fig. 1.9). The slab surface temperature of the subducting slab in the Izu–Bonin subduction zone changed dramatically as subduction evolved and was beyond the wet basalt solidus, resulting in partial melting of the oceanic crust (Fig. 1.9a). However, according to the steady-state model calculation, the slab surface temperature did not result in partial melting of the oceanic crust. In the Mariana subduction zone, transient partial melting of oceanic crust occurred from ca. 40–30 Ma, but this was not observed in the steady-state model experiment (Fig. 1.9b).

Because of the old plate age in the northeast Japan and Kuril subduction zones, partial melting of oceanic crust may not be expected in these subduction zones (e.g., Defant and Drummond, 1990). However, partial melting of the subducting slab likely occurred in the northeast Japan and Kuril subduction zones by ca. 30 Ma and 40 Ma, respectively, resulting in adakitic magmatism in the subduction zones (Figs. 1.9c and 1.9d). In the Tonga subduction zone, slab surface temperature reflects the effects of subduction initiation by ca. 45 Ma (Fig. 1.9e). In the northwestern Java–Sunda subduction zone, slab surface temperature is practically not distinguishable between the time-evolving and steady-state experiments, but partial melting of oceanic crust would be expected in the southeastern Java–Sunda by ca. 20 Ma, a circumstance not observed in the steady-state model experiment using current subduction parameters (Figs. 1.9f and 1.9g). In the western Aleutian subduction zone, the time-evolving subduction model can explain the extensive partial melting of the subducting oceanic crust, although the steady-state model calculations also indicate partial melting of

oceanic crust (Fig. 1.9h). In contrast to the western Aleutians, no remarkable differences are observed in slab surface temperature between the time-evolving and steady-state model calculations for the eastern Aleutians, indicating that the effect of time-evolving subduction parameters is not significant (Fig. 1.9i).

As shown in Fig. 1.9, the time-evolving slab age and convergence rate are likely responsible for the partial melting of the oceanic crust resulting in adakites and boninites in the Izu–Bonin and western Aleutians. Although the steady-state model calculations indicate partial melting of the oceanic crust in the western Aleutians, the time-evolving model calculations highlight the effects of time-evolving subducting parameters on the partial melting of the oceanic crust. This finding indicates that time-evolving subduction parameters should be considered in studies of transient partial melting of the subducting oceanic crust, especially when the subduction parameters have evolved greatly through time.

1.4.2. Other possible mechanisms responsible for adakites and boninites in arc volcanoes in the IBM, northeast Japan, Tonga, and southeastern Java–Sunda subduction zones

Our numerical model calculations including time-evolving subduction parameters successfully explained adakites and boninites in arc volcanoes in the Izu–Bonin and western Aleutians. However, geochemical and petrological observations in the Mariana, northeast Japan, Tonga, and southeastern Java–Sunda subduction zones were not consistent with our model calculations, indicating that other mechanisms not considered in our numerical models are relevant to the adakites and boninites in the arc

volcanoes. In our numerical models, we did not consider the effects of time-evolving regional tectonic processes such as back-arc spreading, mantle plumes, and slab windows resulting from ridge subduction. Previous geochemical and petrological studies (e.g., Falloon et al., 2008; Pearce et al., 1992) have suggested that regional tectonic processes increase mantle temperature and then cause the partial melting of the oceanic crust in the IBM, northeast Japan, Tonga, and southeastern Java–Sunda subduction zones. Therefore, we explore other possible mechanisms that could explain the geochemical and petrological observations in subduction zones located in the IBM, northeast Japan, Tonga, and southeastern Java–Sunda, as summarized in Table 1.1.

1.4.2.1. Izu–Bonin

Although our model results could explain the occurrence of the boninites in the Izu–Bonin subduction zone (Figs. 1.3d and 1.9a), some geochemical studies have suggested that the boninitic volcanism is associated with the Eocene initiation of the IBM subduction (e.g., Ishizuka et al., 2006; Pearce et al., 1992). Pearce et al. (1992) proposed that the boninites in the Izu–Bonin subduction zone were generated by decompression melting due to adiabatic upwelling of depleted mantle during Eocene forearc extension. Stern and Bloomer (1992) also argued that the forearc of the Izu–Bonin subduction zone experienced strong extension during the early magmatism, and that this extensional signature in the forearc was created by subsidence and subsequent retreat of the subducting plate as subduction began. They also suggested that arc volcanism in the Izu–Bonin subduction zone was exceptionally broad (width of arc volcanism: ~200 km) and that early arc magmatism was more extensive than later arc magmatism. Using a numerical model, Hall et al. (2003) found that the Eocene

subduction initiation was accompanied by strong forearc extension, which allowed considerable partial melting in the Izu–Bonin subduction zone. Although our model does not consider extension of the overriding plate, our numerical model calculations sufficiently explain the slab melting required for the boninite occurrences in the Izu–Bonin subduction zone (Fig. 1.3d).

1.4.2.2. Mariana

Our model calculations suggested the possibility of partial melting of subducting oceanic crust from ca. 40–30 Ma in the Mariana subduction zone (Figs. 1.3e and 1.9b). Based on geochemical and petrological studies, late Eocene to early Oligocene boninites drilled from the Mariana forearc (DSDP 458) are consistent with our model calculations (Bloomer, 1987). However, based on the Early Eocene boninites (45–49 Ma) dredged from the inner trench wall, the partial melting of the oceanic crust in the Mariana is not consistent with our model calculations (Fig. 1.3e).

The occurrence of the Early Eocene boninites is related to the rapid extension of the overriding plate during the subduction initiation in the Mariana (~49–48 Ma) (Hall et al., 2003; Pearce et al., 1992; Stern and Bloomer, 1992). In the subduction initiation stage of the Mariana, the young overriding plate was under strong extensional stress and upwelling of the hot asthenospheric mantle that was injected into the mantle wedge may have resulted in higher slab temperatures as well as thinning of the subducting slab. Thus, slab temperatures may have been higher than those our model calculations, thus generating boninites in the Mariana (Pearce et al., 1992; Stern and Bloomer, 1992). Our model calculations indicate that the abnormal Eocene boninites

are attributable to strong extension in the overriding plate and upwelling of the hot asthenospheric mantle that was injected into the mantle wedge during subduction initiation.

1.4.2.3. Northeast Japan

The occurrence of adakites (e.g., Abukuma adakites) in northeast Japan during the Early Miocene (ca. 16 Ma) is not consistent with our model calculations because partial melting of the oceanic crust was reduced significantly since 30 Ma (Figs. 1.5d and 1.9c). However, solid evidence indicates that partial melting of oceanic crust occurred during the Early Miocene at ~16 Ma (Hanyu et al., 2006; Yamamoto and Hoang, 2009). The partial melting of the oceanic crust during the Early Miocene is thought to be attributable to hot asthenospheric mantle injected into the mantle wedge as a result of the opening of the East (Japan) Sea from Early to Late Miocene (Yamamoto and Hoang, 2009). Lee and Lim (2014) suggested an alternative mechanism: a dragged blob of mantle plume that penetrated through the subducted Pacific plate into the corner of the mantle wedge, resulting in partial melting of the oceanic crust. Except for the transient (pulse-like) adakites at ca. 16 Ma, the paucity of partial melting of oceanic crust (Hanyu et al., 2006; Yamamoto and Hoang, 2009) is consistent with our numerical model calculations. The thermal evolution of the Kuril subduction zone, very similar to the northeast Japan subduction zone, suggests that transient (pulse-like) Abukuma adakites are related to the injection of a hot blob of the penetrated mantle plume into the mantle wedge.

1.4.2.4. Tonga

In the Tonga subduction zone, two representative high-Ca boninites and adakites have been recovered. One is the high-Ca boninites from the northern end of the Tonga trench, a transitional boundary from convergent to transform (Danyushevsky et al., 1995; Falloon et al., 2008; Meffre et al., 2012) (Fig. 1.6a). The ages of these northern Tonga boninites are estimated at ~0.5–3 Ma and ~15.2 Ma (Falloon et al., 2008; Meffre et al., 2012), which appear consistent with the slab melting in our model calculations. However, geochemical and experimental studies (Danyushevsky et al., 1994) have estimated the depth for genesis of the high-Ca boninites in the northern Tonga arc at ~45–55 km, much shallower than the depth (~80–100 km) from our model calculations. Additionally, the high-Ca boninites of the Tonga arc are different from the low-Ca boninites at the IBM subduction zone (Cooper et al., 2010; Danyushevsky et al., 1995). The high-Ca boninites reflect a less depleted mantle source than that of the low-Ca boninites (Falloon et al., 1989). Crawford et al. (1989) and Falloon and Crawford (1991) suggested that the enriched component of the high-Ca boninites in the northern Tonga resulted from interaction between a mantle plume and the subducting slab in the transition zone from trench to transform fault. Therefore, it is difficult for our model to explain the genesis of the high-Ca boninites in the northern Tonga.

The high-Ca boninites as well as the adakites recovered in the northern Tonga trench formed at ~2.5 Ma (Falloon et al., 2008). The northern Tonga adakites provide strong geochemical evidence, consistent with their Sr and Nd isotopic compositions, indicating that they resulted from partial melting of oceanic crust (Falloon et al., 2008). However, these have been discovered in the transition zone from the trench to transform fault, which is irrelevant to our model scheme. Therefore, our model

calculations cannot explain the genesis of the northern Tonga adakites.

The other high-Ca boninites of ~1 Ma have been reported in the active Tonga arc, east of the Eastern Lau Spreading Center (Acland, 1996; Cooper et al., 2010), which is consistent with our model results (Fig. 1.6c). However, these boninites are considered to have formed under lower pressure (~30 km) and temperature (~1175–1285°C) than the northern Tonga high-Ca boninites (Cooper et al., 2010), so they are much shallower than our model results (80–100 km). With regard to the boninites in the northern Tonga arc, our model calculations cannot explain the origin of the boninites in the Tonga subduction zone because of the depth inconsistency in the genesis of the high-Ca boninites between geochemical evaluation and our model calculations. Cooper et al. (2010) insisted that the genesis of the high-Ca boninites in the central Tonga arc can be explained by two steps of melting: early melting that occurred in the Lau back-arc basin, and subsequent mantle remelting with slab-derived fluids flowing beneath the arc. Therefore, the high-Ca boninites in the Tonga subduction zone cannot be explained by simple interaction between the subducting slab and overlying mantle wedge, meaning that additional tectonic processes such as back-arc spreading and a mantle plume are required for genesis of the boninites.

1.4.2.5. Southeastern Java–Sunda

Our model calculations indicate partial melting of the oceanic crust in the southeastern Java–Sunda subduction zone occurred from ca. 50 to 20 Ma resulting from Wharton ridge subduction (Fig. 1.7e). However, a lack of ocean drilling and field data in the Java–Sunda subduction zones prevents verification of our model

calculations. Whittaker et al. (2007) proposed that a slab window opened by subduction of the Wharton Ridge underlying the southeastern Java–Sunda from 70–40 Ma, and other studies have concluded that the ridge subduction allowed upwelling of a mantle plume into the shallow mantle, resulting in intrusions of A-type granitoids and adakites above the slab edge (e.g., Kinoshita, 1995, 2002). Although our model calculations represent the ridge subduction as high surface slab temperatures without considering the upwelling of hot asthenosphere, slab temperatures were sufficiently high to generate adakites in the southeastern Java–Sunda by partial melting of the slab edge from ca. 50 to 20 Ma.

Researchers have recovered adakitic rocks with high Sr/Y and La/Yb ratios and low Y and Yb contents similar to the adakites produced by processes other than the partial melting of oceanic crust (e.g., Chung et al., 2003; Hou et al., 2004; Yumul et al., 1999). Castillo (2006) suggested that such adakitic rocks are generated by low-pressure crystal fractionation of amphibole-bearing basaltic magma. Because the thickness of overriding continental crust in the southeastern Java–Sunda is thin (~40 km from gravity modeling) (Grememeyer and Tiwari, 2006), partial melting of the overriding continental crust may not be expected. More detailed geochemical investigation including trace element and radiogenic isotope analyses are needed to verify our model calculations.

1.4.3. Caveats: mantle potential temperature and down-dip treatment in our model calculations

Despite mantle potential temperature being an important controlling factor for

the melting process in subduction zones (Asimow and Langmuir, 2003), this issue has been debated for years. McKenzie and Bickle (1988) proposed that the average potential temperature beneath a ridge is 1280°C, but recent studies based on crustal thickness and thermodynamic models have suggested higher mantle temperatures, ranging from 1350–1450°C (Asimow et al., 2001; Putirka et al., 2007). In our model, we assumed a mantle potential temperature of 1450°C, which is the near upper limit of reported mantle potential temperature. The higher mantle potential temperature may result in easier slab melting, such as a small amount of partial melting of the subducting slab in the eastern Aleutians. However, we did not consider excess heat due to viscous dissipation, which would lead to a thinner thermal boundary layer on the subducting slab and higher slab temperatures. Lee and King (2009) reported that viscous dissipation results in a temperature increase of 50°C at a depth of 100 km. Thus, using a higher mantle potential temperature can be a simple way to consider the effect of viscous dissipation, and this justifies the higher mantle potential temperature used in our model calculations. Next, our model assumed a down-dip depth of the rigid corner of 50 km, which is shallower than that used in other numerical studies (70–80 km) (e.g., Syracuse et al., 2010; Wada and Wang, 2009). The shallow depth of down-dip extent may allow hot material to be dragged into the corner of the mantle wedge, leading to hotter slab temperatures. Thus, our model calculations could be considered as end-member experiments for easier partial melting of the subducting slab.

1.5. Summary

We formulated a series of two-dimensional numerical subduction models using the time-evolving age and convergence rate of the incoming oceanic plate to

understand the genesis of adakites and boninites in the IBM, northeast Japan, Kuril, Tonga, Java–Sunda, and Aleutian subduction zones. Our model calculations successfully explained the adakites and boninites in the Izu–Bonin and Aleutian subduction zones, which cannot be explained by steady-state subduction models using current slab age and convergence rate. However, partial melting of the subducting slab in the Mariana, northeast Japan, Tonga, and southeastern Java–Sunda subduction zones remains unresolved. Our model calculations can be summarized as follows.

(1) Izu–Bonin: Partial melting of oceanic crust is possible from ca. 50 to 25 Ma, consistent with the occurrence of Middle Eocene boninites in the Izu–Bonin arc.

(2) Mariana: Partial melting of oceanic crust is expected from ca. 40 to 30 Ma. The boninites from the Late Eocene to Early Oligocene are consistent with our model calculations, but the Middle Eocene boninites (45–49 Ma) are not. The occurrence of Middle Eocene boninites in the Mariana arc might be related to rapid extension of the overriding plate and upwelling of hot asthenospheric mantle during subduction initiation.

(3) Northeast Japan: Our model calculations show slab melting from 50 to 30 Ma but no slab melting from 30 Ma. These calculations do not explain the occurrence of ca. 16 Ma adakites in the Abukuma region. Thus, the injection of a hot blob from mantle plume that penetrated through the subducting slab may be responsible for the short-term pulse of Abukuma adakites.

(4) Kuril: According to our model calculations, no partial melting of oceanic crust occurred after ca. 40 Ma, which is consistent with the paucity of slab melting in the

region.

(5) Tonga: Partial melting of oceanic crust occurred intermittently during the Quaternary and Middle Miocene, which is well consistent with our model calculations. However, the estimated depth from geochemical data for genesis of the high-Ca boninites and adakites (~30–50 km) is much shallower than that of our model calculations (80–100 km). Additionally, northern Tonga boninites and adakites are located in the transition zone from trench to transform fault, which differs from our model. The boninites in the Tonga subduction zones are relevant to the initiation of subduction and specific tectonic environments that were not considered in our model calculations.

(6) Java–Sunda: In the northwestern Java–Sunda subduction zone, our model results indicate no partial melting of oceanic crust after 50 Ma, consistent with geochemical/petrological data. In contrast, in the southeastern Java–Sunda, our model calculations indicate that partial melting of oceanic crust was possible from 50 to 20 Ma due to subduction of the Wharton Ridge, but we could not find geochemical data supporting slab melting from 50 to 20 Ma.

(7) Aleutians: Our model calculations for the western Aleutians show that partial melting of oceanic crust occurred extensively after 50 Ma, which is consistent with geochemical/petrological evidence from the western Aleutians. In the eastern Aleutians, slab surface temperature was slightly higher than the solidus of wet basalt, which may not have resulted in extensive partial melting of oceanic crust, consistent with the absence of adakites in the eastern Aleutians.

1.6. References

Acland, A.S., 1996. Magma genesis in the northern Lau Basin, S.W. Pacific. PhD thesis, Durham University.

Asimow, P.D., Hirschmann, M.M., Stolper, E.M., 2001. Calculation of peridotite partial melting from thermodynamic models of minerals and melts, IV. Adiabatic decompression and the composition and mean properties of mid-ocean ridge basalts. Journal of Petrology 42(5), 963-998.

Asimow, P.D., Langmuir, C.H., 2003. The importance of water to oceanic mantle melting regimes. Nature 421(6925), 815-820.

Bailey, J.C., Frolova, T.I., Burikova, I.A., 1989. Mineralogy, geochemistry and petrogenesis of Kurile island-arc basalts. Contributions to Mineralogy and Petrology 102(3), 265-280.

Baitsch-Ghirardello, B., Gerya, T.V., Burg, J.P., 2014. Geodynamic regimes of intra-oceanic subduction: Implications for arc extension vs. shortening processes. Gondwana Research 25(2), 546-560.

Bloomer, S.H., 1987. Geochemical characteristics of boninite- and tholeiite-series volcanic rocks from the Mariana forearc and the role of an incompatible element-enriched fluid in arc petrogenesis. Geological Society of America, Special Paper 215, 151-164.

Brocher, T.M., Parsons, T., Tréhu, A.M., Snelson, C.M., Fisher, M.A., 2003. Seismic evidence for widespread serpentinized forearc upper mantle along the Cascadia margin. Geology 31, 267-270.

Cameron, W.E., Nisbet, E.G., Dietrich, V.J., 1979. Boninites, komatiites and ophiolitic basalts. Nature 280(5723), 550-553.

Castillo, P.R., 2006. An overview of adakite petrogenesis. Chinese Science Bulletin

51(3), 257-268.

Castillo, P.R., 2012. Adakite petrogenesis. Lithos 134-135, 304-316.

Chung, S.-L., Liu, D., Ji, J., Chu, M.-F., Lee, H.-Y., Wen, D.-J., Lo, C.-H., Lee, T.-Y., Qian, Q., Zhang, Q., 2003. Adakites from continental collision zones: Melting of thickened lower crust beneath southern Tibet. Geology 31, 1021-1024.

Cooper, L.B., Plank, T., Arculus, R.J., Hauri, E.H., Hall, P.S., Parman, S.W., 2010. High-Ca boninites from the active Tonga Arc. Journal of Geophysical Research: Solid Earth 115(B10), B10206, doi:10.1029/2009JB006367.

Crawford, A.J., Falloon, T.J., Green, D.H., 1989. Classification, petrogenesis and tectonic setting of boninites. In: Crawford, A.J. (Ed), Boninites and Related Rocks. Unwin Hyman, London, pp. 1-49.

Danyushevsky, L.V., Green, D.H., Falloon, T.J., Sobolev, A.V., 1994. The compositions of anhydrous and H_2O-under-saturated melts in equilibrium with refractory peridotites at 15 and 20 Kb: Implications for high-Ca boninite petrogenesis. Mineralogical Magazine 58A(1), 209-210.

Danyushevsky, L.V., Sobolev, A.V., Falloon, T.J., 1995. North Tongan high-Ca boninite petrogenesis: The role of Samoan plume and subduction zone-transform fault transition. Journal of Geodynamics 20(3), 219-241.

Defant, M.J., Drummond, M.S., 1990. Derivation of some modern arc magmas by melting of young subducted lithosphere. Nature 347(6294), 662-665.

Falloon, T.J., Crawford, A.J., 1991. The petrogenesis of high-calcium boninite lavas dredged from the northern Tonga ridge. Earth and Planetary Science Letters 102(3-4), 375-394.

Falloon, T.J., Green, D.H., McCulloch, M.T., 1989. Petrogenesis of high-Mg and associated lavas from the north Tonga trench. In: Crawford, A.J. (Ed), Boninites and Related Rocks. Unwin Hyman, London, pp. 357-395.

Falloon, T.J., Danyushevsky, L.V., Crawford, A.J., Meffre, S., Woodhead, J.D., Bloomer, S.H., 2008. Boninites and adakites from the northern termination of the Tonga trench: Implications for adakite petrogenesis. Journal of Petrology 49(4), 697-715.

Funiciello, F., Faccenna, C., Giardini, D., Regenauer-Lieb, K., 2003. Dynamics of retreating slabs (part 2): Insights from 3-D laboratory experiments. Journal of Geophysical Research: Solid Earth 108(B4), 2207, doi:10.1029/2001JB000896.

Gertisser, R., Keller, J., 2003. Trace element and Sr, Nd, Pb and O isotope variations in medium-K and high-K volcanic rocks from Merapi volcano, Central Java, Indonesia: Evidence for the involvement of subducted sediments in Sunda arc magma genesis. Journal of Petrology 44(3), 457-489.

Gerya, T.V., Yuen, D.A., 2003. Rayleigh-Taylor instabilities from hydration and melting propel 'cold plumes' at subduction zones. Earth and Planetary Science Letters 212, 47-62.

Grevemeyer, I., Tiwari, V.M., 2006. Overriding plate controls spatial distribution of megathrust earthquakes in the Sunda–Andaman subduction zone. Earth and Planetary Science Letters 251(3-4), 199-208.

Guan, Q., Zhu, D.C., Zhao, Z.D., Dong, G.C., Zhang, L.L., Li, X.W., Liu, M., Mo, X.X., Liu, Y.S., Yuan, H.L., 2012. Crustal thickening prior to 38Ma in southern Tibet: Evidence from lower crust-derived adakitic magmatism in the Gangdese Batholith. Gondwana Research 21(1), 88-99.

Gutscher, M.A., Spakman, W., Bijwaard, H., Engdahl, E.R., 2000. Geodynamics of flat subduction: Seismicity and tomographic constraints from the Andean margin. Tectonics 19(5), 814-833.

Hall, C.E., Gurnis, M., Sdrolias, M., Lavier, L.L., Müller, R.D., 2003. Catastrophic initiation of subduction following forced convergence across fracture zones.

Earth and Planetary Science Letters 212(1-2), 15-30.

Handley, H.K., Turner, S., Macpherson, C.G., Gertisser, R., Davidson, J.P., 2011. Hf-Nd isotope and trace element constraints on subduction inputs at island arcs: Limitations of Hf anomalies as sediment input indicators. Earth and Planetary Science Letters 304, 212-223.

Hanyu, T., Tatsumi, Y., Nakai, S., Chang, Q., Miyazaki, T., Sato, K., Tani, K., Shibata, T., Yoshida, T., 2006. Contribution of slab melting and slab dehydration to magmatism in the NE Japan arc for the last 25 Myr: Constraints from geochemistry. Geochemistry, Geophysics, Geosystems 7(8),doi:10.1029/2005GC001220.

Heine, C., Müller, R.D., Gaina, C., 2004. Reconstructing the lost eastern Tethys ocean basin: Convergence history of the SE Asian margin and marine gateways. In: Clift, P., Wang, P., Kuhnt, W., Hayes, D. (Eds), Continent-Ocean Interactions within East Asian Marginal Seas. American Geophysical Union Monograph 149, Washington, pp. 37-54.

Hickey-Vargas, R., Roa, H.M., Escobar, L.L., Frey, F.A., 1989. Geochemical variations in Andean basaltic and silicic lavas from the Villarrica-Lanin volcanic chain (39.5°S): An evaluation of source heterogeneity, fractional crystallization and crustal assimilation. Contributions to Mineralogy and Petrology 103(3), 361-386.

Honda, S., Saito, M., 2003. Small-scale convection under the back-arc occurring in the low viscosity wedge. Earth and Planetary Science Letters 216, 703-715.

Hou, Z.Q., Gao, Y.F., Qu, X.M., Rui, Z.Y., Mo, X.X., 2004. Origin of adakitic intrusives generated during mid-Miocene east-west extension in southern Tibet. Earth and Planetary Science Letters 220, 139-155.

Ishizuka, O., Kimura, J.I., Li, Y.B., Stern, R.J., Reagan, M.K., Taylor, R.N., Ohara, Y., Bloomer, S.H., Ishii, T., Hargrove, U.S., Haraguchi, S., 2006. Early stages in the

evolution of Izu–Bonin arc volcanism: New age, chemical, and isotopic constraints. Earth and Planetary Science Letters 250(1-2), 385-401.

Karato, S., Wu, P., 1993. Rheology of the upper mantle: A synthesis. Science 260(5109), 771-778.

Kay, R.W., 1978. Aleutian magnesian andesites: Melts from subducted Pacific ocean crust. Journal of Volcanology and Geothermal Research 4(1-2), 117-132.

Kay, R.W., Kay, S.M., 1993. Delamination and delamination magmatism. Tectonophysics 219, 177-189.

Kay, S.M., Godoy, E., Kurtz, A., 2005. Episodic arc migration, crustal thickening, subduction erosion, and magmatism in the south-central Andes. Geological Society of America Bulletin 117(1-2), 67-88.

Kelemen, P.B., Yogodzinski, G.M., Scholl, D.W., 2003. Along-strike variation in the Aleutian island arc: Genesis of high Mg# andesite and implications for continental crust. In: Eiler, J. (Ed), Inside the Subduction Factory. American Geophysical Union Monograph 138, Washington, pp. 223-276.

Kessel, R., Ulmer, P., Pettke, T., Schmidt, M.W., Thompson, A.B., 2005. The water-basalt system at 4 to 6 GPa: Phase relations and second critical endpoint in a K-free eclogite at 700 to 1400 degrees C. Earth and Planetary Science Letters 237(3-4), 873-892.

Kincaid, C., Druken, K.A., Griffiths, R.W., Stegman, D.R., 2013. Bifurcation of the Yellowstone plume driven by subduction-induced mantle flow. Nature Geoscience 6, 395-399.

King, S.D., Raefsky, A., Hager, B.H., 1990. Vectorizing a finite element code for incompressible two-dimensional convection in the Earth's mantle. Physics of the Earth and Planetary Interiors 59, 195-207.

Kinoshita, O., 1995. Migration of igneous activities related to ridge subduction in

Southwest Japan and the East Asian continental margin from the Mesozoic to the Paleogene. Tectonophysics 245(1-2), 25-35.

Kinoshita, O., 2002. Possible manifestations of slab window magmatisms in Cretaceous southwest Japan. Tectonophysics 344(1-2), 1-13.

Koto, B., 1916. On the volcanoes of Japan (V). The Journal of the Geological Society of Japan 23, 95-127.

Krishna, K.S., Rao, D.G., Ramana, M.V., Subrahmanyam, V., Sarma, K., Pilipenko, A.I., Shcherbakov, V.S., Murthy, I.V.R., 1995. Tectonic model for the evolution of oceanic crust in the northeastern Indian Ocean from the Late Cretaceous to the Early Tertiary. Journal of Geophysical Research: Solid Earth 100(B10), 20011-20024, doi:10.1029/94JB02464.

Kuroda, N., Shiraki, K., Urano, H., 1978. Boninite as a possible calc-alkalic primary magma. Bulletin of Volcanology 41(4), 563-575.

Lai, S.C., Qin, J.F., 2013. Adakitic rocks derived from the partial melting of subducted continental crust: Evidence from the Eocene volcanic rocks in the northern Qiangtang block. Gondwana Research 23(2), 812-824.

Lee, C., King, S.D., 2009. Effect of mantle compressibility on the thermal and flow structures of the subduction zones. Geochemistry, Geophysics, Geosystems 10(1), Q1006, doi:10.1029/2008GC002151.

Lee, C., King, S.D., 2010. Why are high-Mg# andesites widespread in the western Aleutians? A numerical model approach. Geology 38(7), 583-586.

Lee, C., King, S.D., 2011. Dynamic buckling of subducting slabs reconciles geological and geophysical observations. Earth and Planetary Science Letters 312(3-4), 360-370.

Lee, C., Lim, C., 2014. Short-term and localized plume-slab interaction explains the genesis of Abukuma adakite in Northeastern Japan. Earth and Planetary Science

Letters 396, 116-124.

Lee, C., Ryu, I.-C., A new tectonic model for the genesis of adakitic arc magmatism in Cretaceous East Sea. American Geophysical Union Monograph, Washington, accepted.

Macpherson, C.G., Hall, R., 2001. Tectonic setting of Eocene boninite magmatism in the Izu–Bonin–Mariana forearc. Earth and Planetary Science Letters 186(2), 215-230.

Martynov, Y.A., Khanchuk, A.I., Kimura, J.I., Rybin, A.V., Martynov, A.Y., 2010. Geochemistry and petrogenesis of volcanic rocks in the Kuril island arc. Petrology 18(5), 489-513.

Martynov, Y.A., Kimura, J.I., Martynov, A.Y., Rybin, A.V., Katakuse, M., 2012. Indian MORB-type mantle beneath the Kuril Island arc: Isotopic investigation of the mafic lavas of Kunashir Island. Petrology 20(1), 93-100.

Maruyama, S., Liou, J.G., Terabayashi, M., 1996. Blueschists and eclogites of the world and their exhumation. International Geology Review 38, 485-594.

McKenzie, D., Bickle, M.J., 1988. The volume and composition of melt generated by extension of the lithosphere. Journal of Petrology 29(3), 625-679.

Meffre, S., Falloon, T.J., Crawford, T.J., Hoernle, K., Hauff, F., Duncan, R.A., Bloomer, S.H., Wright, D.J., 2012. Basalts erupted along the Tongan fore arc during subduction initiation: Evidence from geochronology of dredged rocks from the Tonga fore arc and trench. Geochemistry, Geophysics, Geosystems 13(12), Q12003, doi:10.1029/2012GC004335.

Mibe, K., Kawamoto, T., Matsukage, K.N., Fei, Y., Ono, S., 2011. Slab melting versus slab dehydration in subduction-zone magmatism. Proceedings of the National Academy of Science of the United States of America 108(20), 8177-8182.

Nichols, G.T., Wyllie, P.J., Stern, C.R., 1994. Subduction zone melting of pelagic

sediments constrained by melting experiments. Nature 371(6500), 785-788.

Peacock, S.M., 1996. Thermal and petrologic structure of subduction zones. In: Bebout, G.E., Scholl, D.W., Kirby, S.H., Platt, J.P. (Eds), Subduction: Top to Bottom. American Geophysical Union Monograph 96, Washington, pp. 119-133.

Pearce, J.A., van der Laan, S.R., Arculus, R.J., Murton, B.J., Ishii, T., Peate, D.W., Parkinson, I.J., 1992. Boninite and Harzburgite from leg 125 (Bonin-Mariana Forearc): A case study of magma genesis during the initial stages of subduction. In: Fryer, P., Coleman, P., Pearce, J.A., Stokking, L.B. (Eds), Proceedings of the Ocean Drilling Program, Scientific Results 125, Texas A&M University, pp. 623-659.

Pedersen, R.B., Searle, M.P., Carter, A., Bandopadhyay, P.C., 2010. U-Pb zircon age of the Andaman ophiolite: Implications for the beginning of subduction beneath the Andaman-Sumatra arc. Journal of the Geological Society 167(6), 1105-1112.

Putirka, K.D., Perfit, M., Ryerson, F.J., Jackson, M.G., 2007. Ambient and excess mantle temperatures, olivine thermometry, and active vs. passive upwelling. Chemical Geology 241(3-4), 177-206.

Richards, J.P., Kerrich, R., 2007. Special paper: Adakite-like rocks: Their diverse origins and questionable role in metallogenesis. Economic Geology 102, 537-576.

Rogers, G., Saunders, A.D., Terrell, D.J., Verma, S.P., Marriner, G.F., 1985. Geochemistry of Holocene volcanic rocks associated with ridge subduction in Baja California, Mexico. Nature 315(6018), 389-392.

Sato, H., 1994. The relationship between Late Cenozoic tectonic events and stress field and basin development in northeast Japan. Journal of Geophysical Research: Solid Earth 99(B11), 22261-22274, doi:10.1029/94JB00854.

Saunders, A.D., Rogers, G., Marriner, G.F., Terrell, D.J., Verma, S.P., 1987.

Geochemistry of Cenozoic volcanic rocks, Baja California, Mexico: Implications for the petrogenesis of post-subduction magmas. Journal of Volcanology and Geothermal Research 32(1-3), 223-245.

Schmidt, M.W., Poli, S., 1998. Experimentally based water budgets for dehydrating slabs and consequences for arc magma generation. Earth and Planetary Science Letters 163(1-4), 361-379.

Sdrolias, M., Müller, R.D., 2006. Controls on back-arc basin formation. Geochemistry, Geophysics, Geosystems 7(4), Q04016, doi:10.1029/2005GC001090.

Stein, C.A., Stein, S., 1992. A model for the global variation in oceanic depth and heat flow with lithospheric age. Nature 359(6391), 123-129.

Stern, R.J., Bloomer, S.H., 1992. Subduction zone infancy: Examples from the Eocene Izu–Bonin–Mariana and Jurassic California arcs. Geological Society of America Bulletin 104(12), 1621-1636.

Stern, C.R., Kilian, R., 1996. Role of the subducted slab, mantle wedge and continental crust in the generation of adakites from the Andean Austral volcanic zone. Contributions to Mineralogy and Petrology 123(3), 263-281.

Stern, R.A., Hanson, G.N., Shirey, S.B., 1989. Petrogenesis of mantle-derived, LILE-enriched Archean monzodiorites and trachyandesites (sanukitoids) in southwestern Superior Province. Canadian Journal of Earth Sciences 26(9), 1688-1712.

Straub, S.M., Zellmer, G.F., 2012. Volcanic arcs as archives of plate tectonic change. Gondwana Research 21(2-3), 495–516.

Syracuse, E.M., Abers, G.A., 2006. Global compilation of variations in slab depth beneath arc volcanoes and implications. Geochemistry, Geophysics, Geosystems 7(5), Q05017, doi:10.1029/2005GC001045.

Syracuse, E.M., van Keken, P.E., Abers, G.A., 2010. The global range of subduction

zone thermal models. Physics of the Earth and Planetary Interiors 51(8), 1761–1782, doi:10.1016/j.pepi.2010.02.004.

Tatsumi, Y., Ishizaka, K., 1981. Existence of andesitic primary magma: An example from southwest Japan. Earth and Planetary Science Letters 53(1), 124-130.

Tatsumi, Y., Otofuji, Y.I., Matsuda, T., Nohda, S., 1989. Opening of the Sea of Japan back-arc basin by asthenospheric injection. Tectonophysics 166(4), 317-329.

van Keken, P.E., Kiefer, B., Peacock, S.M., 2002. High-resolution models of subduction zones: Implications for mineral dehydration reactions and the transport of water into the deep mantle. Geochemistry, Geophysics, Geosystems 3(10), 1056, doi:10.1029/2001GC000256.

Wada, I., Wang, K., 2009. Common depth of slab–mantle decoupling: Reconciling diversity and uniformity of subduction zones. Geochemistry, Geophysics, Geosystems 10, Q10009, doi:10.1029/2009GC002570.

Whittaker, J.M., Miffler, R.D., Sdrolias, M., Heine, C., 2007. Sunda-Java trench kinematics, slab window formation and overriding plate deformation since the Cretaceous. Earth and Planetary Science Letters 255(3-4), 445-457.

Yamamoto, T., Hoang, N., 2009. Synchronous Japan Sea opening Miocene fore-arc volcanism in the Abukuma Mountains, NE Japan: An advancing hot asthenosphere flow versus Pacific slab melting. Lithos 112(3-4), 575-590.

Yogodzinski, G.M., Kelemen, P.B., 1998. Slab melting in the Aleutians: Implications of an ion probe study of clinopyroxene in primitive adakite and basalt. Earth and Planetary Science Letters 158(1-2), 53-65.

Yumul, G.P.Jr, Dimalanta, C.B., Faustino, D.V., de Jesus, J.V., 1999. Silicic arc volcanism and lower crust melting: An example from the central Luzon, Philippines. Journal of Geology 154, 13-14.

1.7. Figures

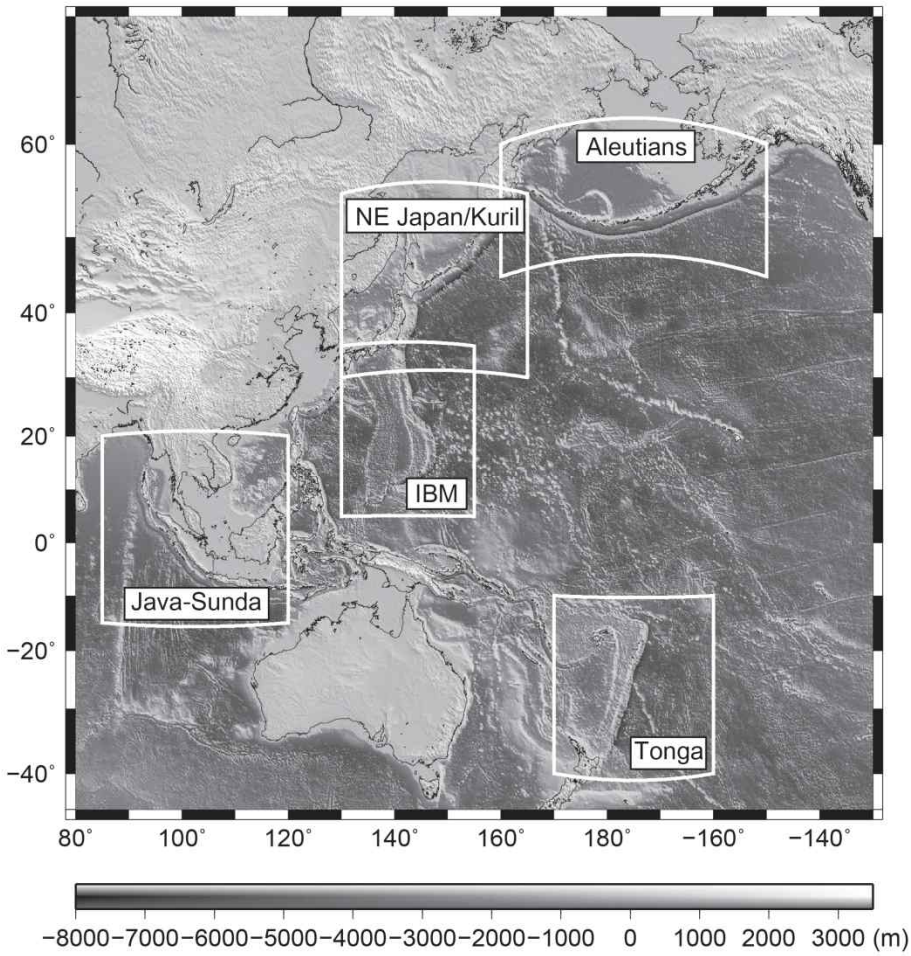

Figure 1.1 Bathymetric map (ETOPO2: Global digital elevation model derived from the National Geophysical Data Center (NGDC)) of the eastern Indian Ocean and western Pacific Ocean including our study areas: Izu–Bonin–Mariana (IBM), northeast Japan–Kuril, Tonga, Java–Sunda, and Aleutian subduction zones (white boxes).

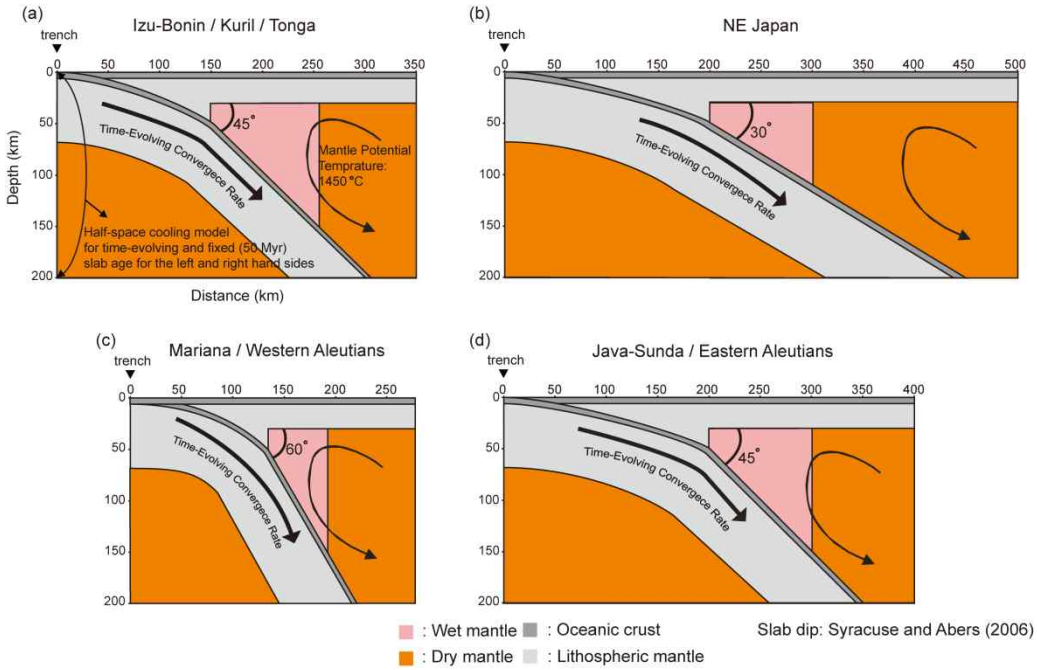

Figure 1.2 Schematic diagrams indicating the subduction models for the (a) Izu–Bonin/Kuril/Tonga, (b) Mariana, (c) northeast Japan/western Aleutians, and (d) Java–Sunda/eastern Aleutians, respectively. The arrows indicate the direction of subduction to the trench. The geometries of the subduction zones are based on Syracuse and Abers (2006). The mantle wedge above the subducting slab is considered to have wet olivine rheology to 150 km. For the asthenospheric mantle excluding the hydrated mantle wedge, we use dry olivine rheology. Dark and light-gray shading indicate oceanic crust and lithospheric mantle, respectively. We assumed that the crust of the overriding plate is oceanic because the overriding plates of the subduction zones considered in our model, except for the Java–Sunda subduction zone, are oceanic plates. The corner flow described on the panels is schematic and the detailed mantle flow is determined by viscous coupling between the mantle and subducting slab (see Fig. 1.4.).

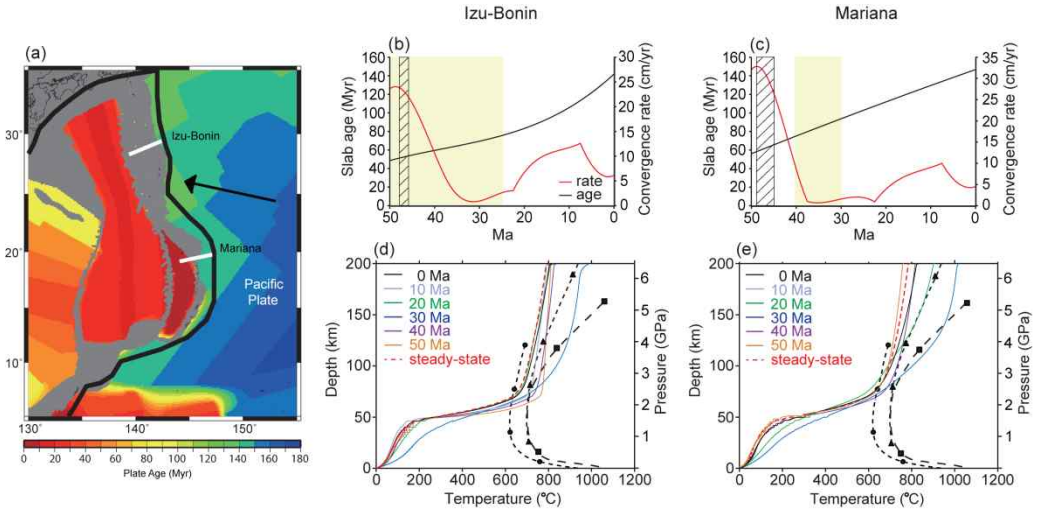

Figure 1.3 (a) Schematic map of the current Izu–Bonin and Mariana subduction zones with major plate boundaries (black lines). The present plate age grid is based on Sdrolias and Müller (2006). The two white lines indicate the locations of the two representative subduction models, and relative plate motion is shown by the black arrow. (b–c) Time-evolving age and convergence rate of the subducting plate in the Izu–Bonin and Mariana subduction zones. Yellow shading denotes the possible period of slab melting from our model calculations, and diagonal-line shading indicates the age of adakites or boninites from geochemical observations. (d–e) Depth versus calculated temperature curves from our model calculations. Solid lines correspond to slab surface temperature at every 10 Myr, and the red dotted line represents the temperature from the steady-state model. The black dashed lines represent the low (triangle) and high (square) end-members of wet basalt and the solidus of wet pelagic sediments (circle), respectively.

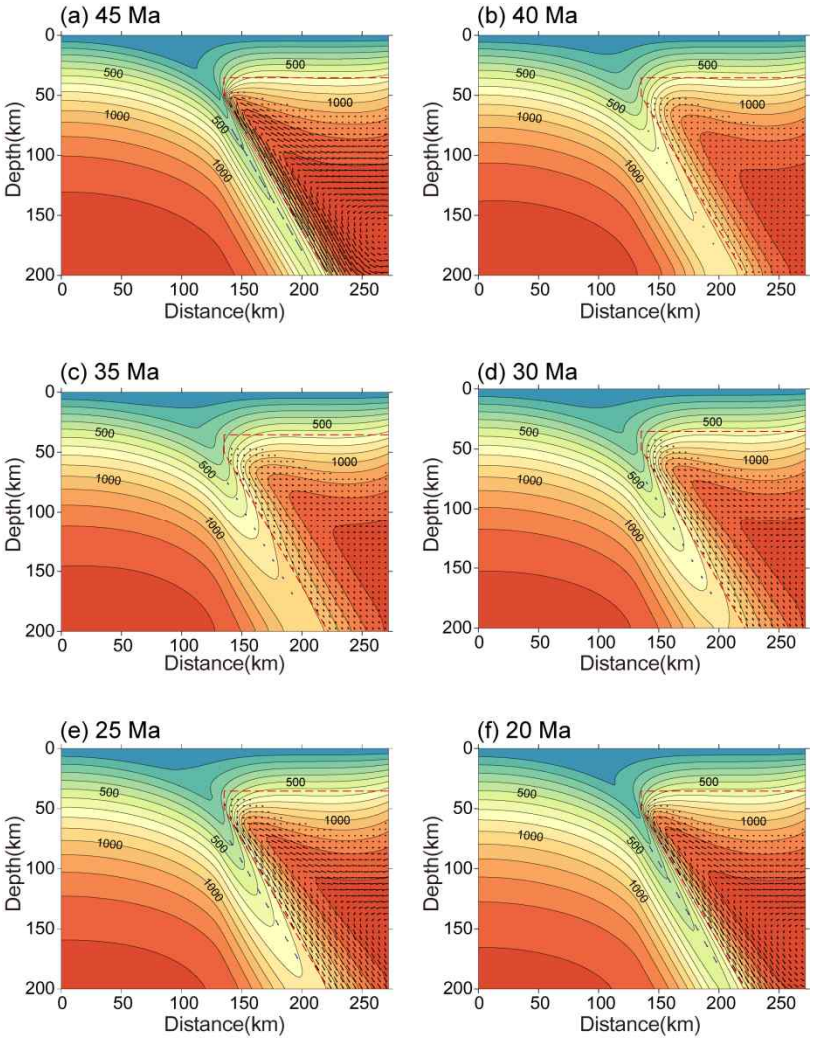

Figure 1.4 Temperature and velocity in the Mariana subduction zone at 45, 40, 35, 30, 25, and 20 Ma. The unit of temperature is degree Celsius (°C), and the contour is drawn at every 100°C. The arrows in the mantle wedge indicate mantle flow velocity. The flows in the mantle wedge are dynamically calculated, and the top and bottom boundaries of the mantle wedge are shown with dashed red lines. The blue arrows denote the convergence rate of the subducting slab.

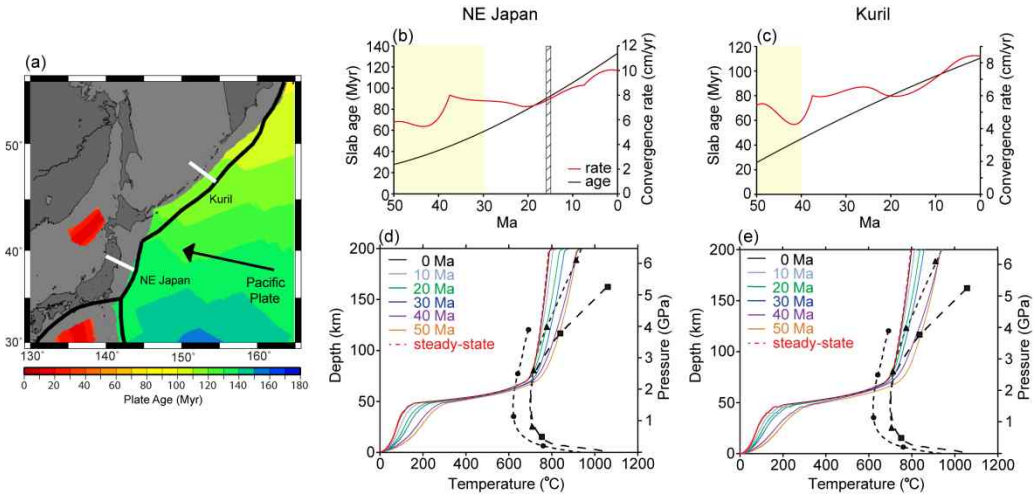

Figure 1.5 (a) Schematic map of the northeast Japan and Kuril subduction zones with major plate boundaries (black lines). (b–c) Time-evolving slab age and convergence rate of the subducting plate in the northeast Japan and Kuril subduction zones. (d–e) Depth versus calculated temperature curves from our model calculations. All shadings, lines, and arrows are the same as in Fig. 1.3.

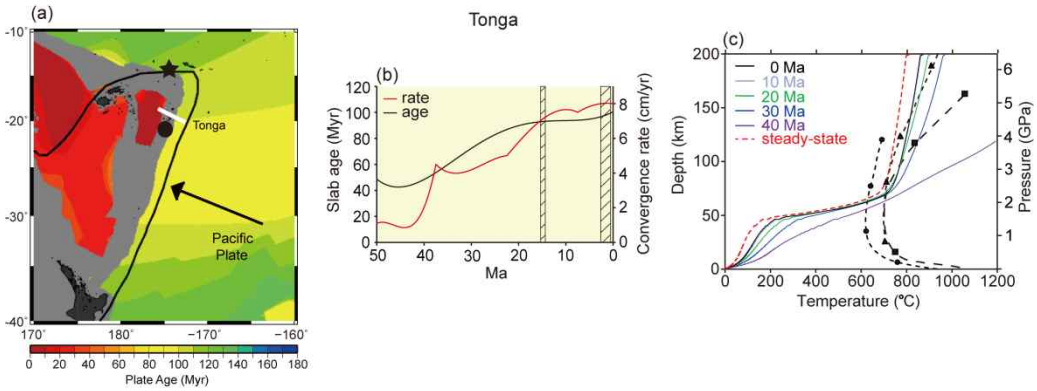

Figure 1.6 (a) Schematic map of the Tonga subduction zone with major plate boundaries (black lines). The black star and circle indicate the locations of the North Tonga adakites/boninites and the boninites from the central portion of the Tonga forearc, respectively. (b) Time-evolving age and convergence rate of the subducting plate at Tonga. (c) Depth versus calculated temperature curves from our model calculations. All shadings, lines, and arrows are the same as in Fig. 1.3.

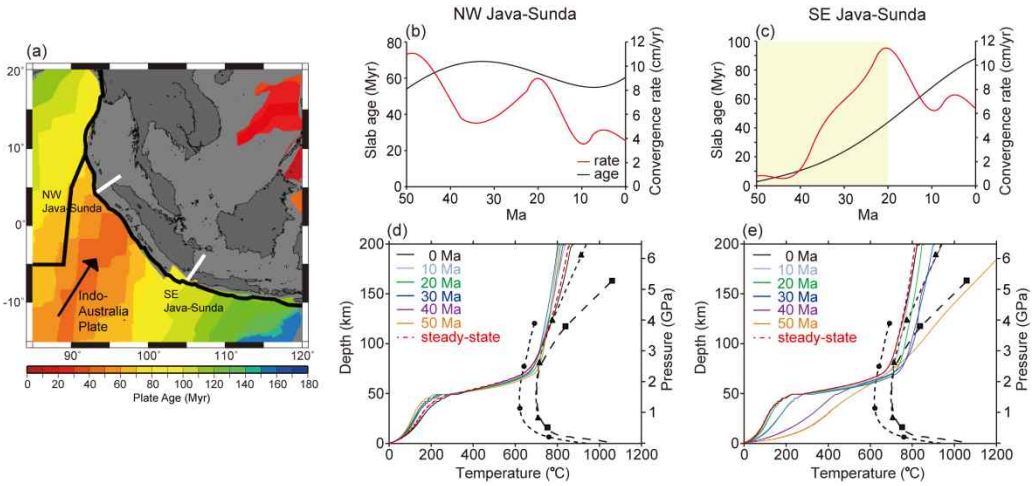

Figure 1.7 (a) Schematic map of the Java–Sunda subduction zone with major plate boundaries (black lines). (b–c) Time-evolving slab age and convergence rate of the subducting plate in the northwestern and southeastern Java–Sunda. (d–e) Depth versus calculated temperature curves from our model. All shadings, lines, and arrows are the same as in Fig. 1.3.

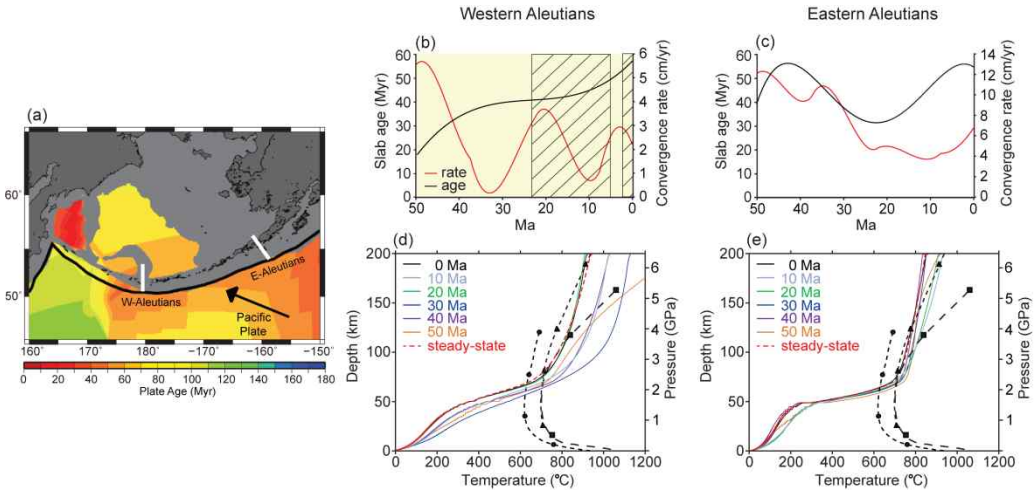

Figure 1.8 (a) Schematic map of the Aleutian subduction zone with major plate boundaries (black lines). (b–c) Time-evolving slab age and convergence rate of the subducting plate in the western and eastern Aleutians. (d–e) Depth versus calculated temperature curves from our model calculations. All shadings, lines, and arrows are the same as in Fig. 1.3.

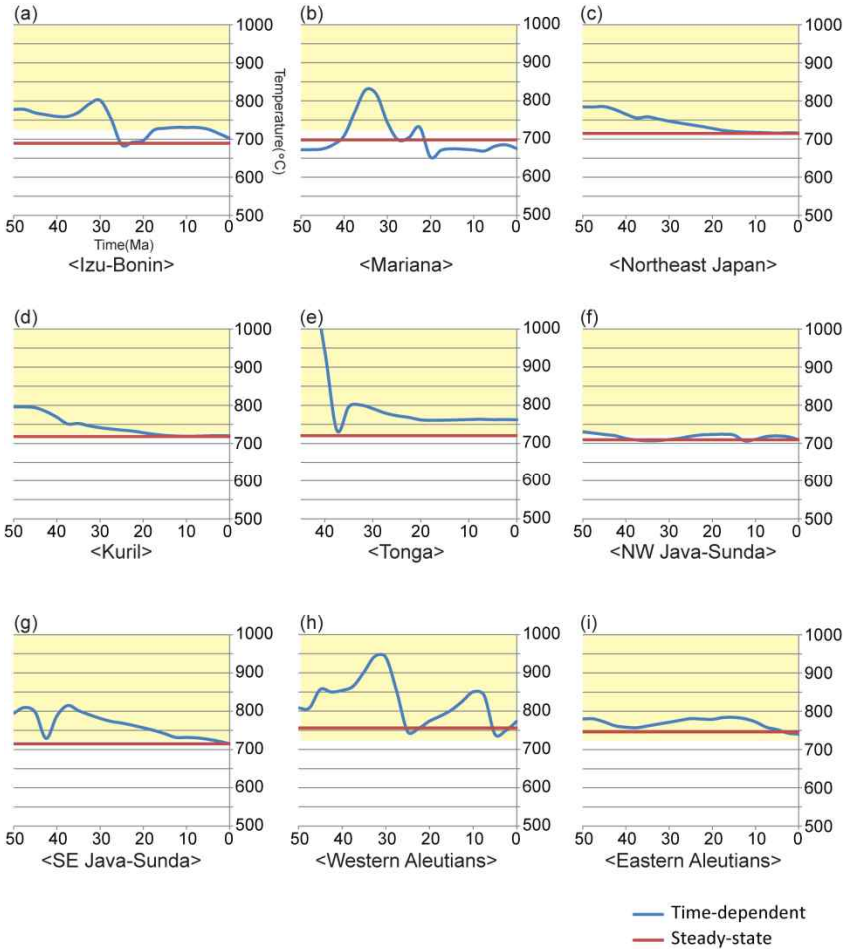

Figure 1.9 Profiles of surface slab temperature at a 90-km depth in our model calculations. The blue and red lines denote slab surface temperatures from the time-dependent and steady-state subduction models, respectively. Yellow shading represents temperature higher than the wet basalt solidus of Schmidt and Poli (1998) at a depth of 90 km, which is a possible region for partial melting of oceanic crust.

1.8. Table

region	Slab melting (our model results)	Slab melting (geochemical observation)	Alternative explanation (relevant references)
Izu-Bonin	50-25 Ma	48-46 Ma	Forearc extension during subduction initiation (Stern & Bloomer 1992)
Mariana	40-30 Ma	49-45 Ma	Forearc extension and upwelling of hot asthenospheric mantle during subduction initiation (Pearce et al. 1992; Stern & Bloomer 1992)
Northeast Japan	50-30 Ma	~16 Ma	Injection of the hot asthenospheric mantle (Hanyu et al. 2006; Yamamoto and Hoang, 2009) or injection of the dragged blob of the mantle plume through the subducted Pacific plate (Lee and Lim, 2014)
Kuril	50-40 Ma	No data	-
Tonga	45 Ma-present	3-0.5 Ma & ~15.2 Ma (boninites) ~2.5 Ma (adakites)	Inconsistent w/t geochemical observation -Boninites and adakites were generated in shallower depth than our model and located in the transition zone differed from our model. (Danyushevsky et al. 1994)
NW Java-Sunda	No slab melting	No data	-
SE Java-Sunda	50-20 Ma	No data	Ridge subduction (Whittaker et al. 2007)
Western Aleutians	50 Ma-present	Miocene and Quaternary	-
Eastern Aleutians	No slab melting	Marginal occurrence of adakites	-

Table 1.1 Comparison of the model calculations with geochemical observations.

Chapter 2

Analysis of marine gravity anomalies in the Ulleung Basin (East Sea/Sea of Japan) and its implications for the architecture of rift-dominated backarc basin

Abstract

Marginal basins locate between the continent and arc islands often exhibit diverse style of opening, from regions that appear to have formed by well-defined and localized spreading center (manifested by the presence of distinct seafloor magnetic anomaly patterns) to those with less obvious zones of extension and a broad magmatic emplacement most likely in the lower crust. Such difference in the style of back-arc basin formation may lead to marked difference in crustal structure in terms of its overall thickness and spatial variations. The Ulleung Basin, one of three major basins in the East Sea/Sea of Japan, is considered to represent a continental rifting end-member of back-arc opening. Although a great deal of work has been conducted on the sedimentary sections in the last several decades, the deep crustal sections have not been systematically investigated for long time, and thus the structure and characteristics of the crust remain poorly understood. This study examines the marine gravity anomalies of the Ulleung Basin in order to understand the crustal structure using crucial sediment-thickness information. Our analysis shows that the Moho depth in general varies from 16 km at the basin center to 22 km at the margins. However, within the basin center, the inferred thickness of the crust is more or less the same (10-12 km), thus by varying only about 10-20% of the total thickness, contrary to the previous impression. The almost-uniformly-thick crust that is thicker than a normal oceanic crust (~ 7 km) is consistent with previous observations using ocean bottom

seismometers and recent deep seismic results from the nearby Yamato Basin. Another important finding is that small residual mantle gravity anomaly highs exist in the northern part of the basin. These highs are aligned in the NNE-SSW direction which corresponds to the orientation of the major tectonic structures on the Korean Peninsula, raising the possibility that, though by a small degree, they are a consequence of localized extension and extra crustal thinning at the time of basin formation. Alternative explanation is that they are the result of small post-rift underplating at the base of the crust. Two important processes appear to have shaped the Ulleung Basin following its formation: post-rifting magmatism which occurred in the north, especially in the northeast sections of the Ulleung Basin, and the deflection of crust in response to preferential sediment loading towards the south. The median high in the basin may be a consequence of the flexural bending. Based on our evidence for almost-uniformly-thick crust, we argue that, unlike many other rift-dominated basins which exhibit large variations in crustal thickness, decompressional melting that took place during basin extension resulted in a widespread magmatic emplacement that not only smoothened but also enhanced the crustal thickness.

Keywords: East Sea, Ulleung Basin, gravity anomaly, crustal thickness, magmatic underplating

2.1. Introduction

Understanding the formation and evolution of back-arc basins at the margin of the continent is an important issue in earth sciences that has significant implications for not only geology itself but also on societal matters as they are the key sites of natural disaster such as earthquakes and volcanoes and the depository of hydrocarbon resources. However, the studies of fundamental processes controlling the development of marginal basins have not been easy because often they are located at the national boundaries and covered by thick sediment.

Back-arc basin exhibits diverse structures and stages of evolution from continental-rift dominated to seafloor-spreading type. In last decades, a great deal of understanding has been made on the latter where sediment thickness is not very large to mask the crustal undulations, including East Scotia Sea (Barker, 1995), Lau Basin (Taylor et al., 1996) and numerous back-arc basins in the Philippine Sea Plate (Okino et al., 1998; Sdrolias et al., 2004). In particular, comparisons were made against mid-ocean ridges. According to Kinsman (1975) and Veevers (1981), back-arc basins develop by splitting the arc and with seafloor spreading the basin widens and the spreading center moves away from the arc. However, it is unclear if such style of development also occurs in the continental-rift dominated cases.

The Ulleung Basin, along with Yamato Basin and Japan Basin, is one of three major basins within East Sea/Sea of Japan. It is considered as a continental-rift dominated type as opposed to Japan Basin which exhibits systematic magnetic anomaly patterns indicative of seafloor spreading. According to Jolivet and Tamaki (1992), the opening in this region has changed from seafloor-spreading style opening

in the northeast (Japan Basin) to continental-rifting style opening in the southwest (Ulleung Basin) during the Late Oligocene to Middle Miocene. Since crustal deformation depends on stress envelop, which in turn is controlled by rheology as a function of material properties, strain rate and temperature, the difference in the opening style is likely to give rise in unique tectonic features that can be observed by deep seismic investigations.

Many seismic studies have been conducted in the Ulleung Basin as part of big national programs in Korea, but only a handful of studies have focused on the deep structure. Unfortunately, even those that imaged the deep structure (Lee et al., 1999; 2001), because of thick sediment which in the southern part exceed 10 km, only the reflection from the top of the crust could be imaged. In recent years, a couple of deep seismic refraction surveys using ocean bottom seismometers have been conducted in the Ulleung Basin (Kim et al., 1998; 2003). However, their coverage was quite limited and we still lack general understanding on the overall structure of the Ulleung Basin.

Another effective way to resolve the crustal structure is the analysis of gravity data. If reliable auxiliary information such as density and sediments thickness (top of the crust) can be used, the interpretation of the gravity anomaly can provide important constraint on the variations of crustal thickness throughout the basin. Our study used the data of sediment thickness acquired from the seismic studies in gravity data reduction, causing to more reliable results of crustal structure in the Ulleung Basin.

This study looks at the gravity anomaly of the Ulleung Basin using various sources of information that has been obtained to date. We examine both gravity data collected by shipboard measurements and anomalies inferred from satellite altimetry

carefully to check how much they differ. In addition, the effect of cooling on the gravity anomaly is investigated by exploring possible changes in stretching factor and mantle potential temperature. Although this is not the first attempt to analyze gravity data of the Ulleung Basin, some of the reduction procedures and subsequent interpretation of gravity anomaly in the previous investigation were ambiguous, conflicting with seismic observations and understanding. It is hoped that our study, by resolving the controversy, will shed new light on the nature of deep crust in the Ulleung Basin and lead to a better understanding of backarc basin formation and evolution.

2.2. Regional Background

The Ulleung Basin is located in the southwestern corner of East Sea/Sea of Japan in the northwestern Pacific (Fig. 2.1a). The basin is bounded on the west by the Korean Peninsula, to the east by continental rifted fragments including Yamato rise, Oki bank and Korean Plateau. A number of volcanoes are distributed in the northeastern part of the basin including Ulleung and Dok islands which have formed during the Late Miocene to the Quaternary (Sohn and Park, 1994; Sohn, 1995).

Figure 2.1b is the bathymetry map of the Ulleung Basin and its vicinity. The water depth reaches at 2000 to 2300 m near the center of the basin. The northern and southern margins appear quite differently; the former is characterized by steep continental fragments and volcanic seamounts, whereas the latter is smooth and covered by thick sediment supplied by the erosion of Japan arc. The sediment is almost 10 km thick at the southern margin of the Ulleung Basin. In addition to the large

variation in sediment thickness, Kim et al. (submitted) recognized other evidences of asymmetric distribution including volcanic and magmatic edifices within the sedimentary layers and in the sub-surface faults near the crustal basement.

Various ideas have been proposed on the opening of East Sea/Sea of Japan over the years (see Yoon et al. (2014) and references therein). However, many of them are more or less similar and not mutually exclusive as they relied on early marine information prior to modern-day investigations and large-scale regional features on land. Important clues for deep structure came from a series of seafloor drilling investigation. The ODP Legs 127 and 128 suggested that the opening of the East Sea/ Sea of Japan commenced at the Late Oligocene and subsequent back-arc spreading until the Middle Miocene (Jolivet et al., 1994). The basement of the Japan Basin comprises calc-alkaline basalt and andesitic lava flows (Ludwig et al., 1975; Honza et al., 1978) with magnetic lineations but the Yamato Basin is covered thick layer of sediment and basaltic-doleritic sill complex differed from the typical oceanic crust (Chough et al., 2000). However, the Ulleung Basin was not visited by the international program, and as a result much of the present-day arguments on the Ulleung Basin need to be validated by future deep sea drilling.

In the last 20 years, the acquisition of high resolution bathymetry, shipborne gravity and total field magnetic data have been instrumental in our understanding of the Ulleung Basin. These data were obtained by various agencies including KHOA (Korea Hydrographic and Oceanographic Agency), KIOST (Korea Institute of Ocean Science and Technology) and KIGAM (Korea Institute of Geoscience and Mineral Resources) with modern research vessels. Also numerous high resolution seismic surveys have been conducted in the basin as part of gas hydrate explorations (Horozal

et al., 2009; Kim et al., 2011b). However, compared to shallow features, very little is understood on the deep structures of the Ulleung Basin.

One of the important data sets that has served as a backbone in the study of deep crustal structure has been KNOC data that has been collected by a Western Geophysical Company seismic vessels in 1988. This data consists of over 2300 km of multi-channel seismic profiles and 120-chnnel streamer recorded shots from 4500-psi airgun array. Most of our understandings of the crustal nature come from this investigation (Lee et al., 1999; 2001). Unfortunately, however, the resulting images only extends to the boundary between sedimentary layer and what appears as the crystalline crust, and thus at best, one can only obtain the information regarding the depth to the top of the crust.

Several wide-angle seismic studies were conducted around the Ulleung Basin using ocean bottom seismometers (Kim et al., 1998; 2003). On the basis of p-wave velocity structure, they argued that the Ulleung Basin is underlain by oceanic crust. However, there are a number of problems with this interpretation. For instance, the argument of Kim et al. (1998) is largely based on the seismic velocity structure in the uppermost part of the crust, which they interpreted as representing the layer 2A (pillow basalt) and layer 2B (sheeted dikes) similar to the oceanic crust produced at mid-ocean ridges. However, recent studies (Christeson et al., 2007; 2010) suggest that the boundary between layer 2A and 2B may not be that of distinct geological units but instead change in the porosity of the uppermost crust as a result of increasing alteration by seawater and filling of the cracks, and thus may not be unique to an oceanic crust. In other words, any new magma extruded on the seafloor and experienced intense interaction with seawater may produce a similar velocity profile on seismic record over

time. Also, the thickness of the crust in the Ulleung Basin (10-15 km) is much higher than that of a normal oceanic crust (7 km). Kim et al. (1998) argue that the melt production was greater in Ulleung Basin than in the normal mid-ocean ridges. However, if magmatic production was indeed robust, it does put the absence of organized magnetic anomaly patterns into a greater doubt.

The lack of well-defined magnetic anomaly patterns and the fact that many intrusive magmatic and volcanic features are found within the sedimentary sequences suggest that the upwelling and outflow of new lava on the seafloor of the Ulleung Basin did not occur at one location like the narrow neo-volcanic zone of the mid-ocean ridges (1-2 km wide) but instead took place at a much wider region or multiple locations in conjunction with tectonic extension. Sato et al. (2006) who conducted deep seismic study using ocean bottom seismometers in the southeastern margin of the Ulleung Basin also interpret the structure of this region as extended continental crust.

The gravity data of the Ulleung Basin was analyzed earlier using shipboard measurements (Park et al., 2006; 2009). However, there are many gaps in KIOST shipboard observations, and thus satellite free-air gravity data were used to cover regions where there were no direct measurements. The analysis of marine gravity data depend very much on the structure beneath the seafloor. The greatest uncertainty arises from the precise definition of sediment thickness (i.e., the boundary between sediment and crust) which varies a lot in the Ulleung Basin. There are also regions where it is difficult to locate the crustal basement because the sediment is too thick.

In the study of Park et al. (2009), sediment thickness within the basin was defined using NGDC data. However, the number of tracklines was small and thus

could pose a problem. Park et al. (2009) suggest a large variation in crustal thickness can be seen in the Ulleung Basin. However, it is somewhat unclear and confusing because the large variation can only be seen in their final diagram and not so much in the corresponding contour plot. In fact, one of the motivations for our study was the apparent disparity between this earlier gravity analysis result and the depth of Moho determined from numerous ocean bottom seismometers studies, which do not exhibit such a large variation in the crustal thickness. Also, most of the previous studies illuminating the origin of the Ulleung Basin do not consider the variation in crustal thickness and therefore, our study focuses on the variation in crustal thickness and its implications on the opening history of the Ulleung Basin.

2.3. Data and Reduction

The study area is delineated in latitude by 35.7-37.8°N and in longitude by 129.8-132°E. The bathymetry data which represents the density boundary between seawater (1.0 g/cm^3) and sediment (2.3 g/cm^3) was acquired by KIGAM in 2000-2014 (Fig. 2.1b). It was constructed using multibeam echo sounder (Simrad EM12S/950). A close examination reveals small north-south streaks in the bathymetry map which are artifacts, presumably resulting from problems in the sound velocity corrections.

The shipboard gravity data in the Ulleung Basin have been obtained by KIGAM from 1997 to 2014 using a LaCoste-Romberg Model-S gravimeter. Its trackline coverage is shown in Figure 2.2a. Gravity data acquired from marine gravimeter has considerable accuracy and has advantage to investigate the small wavelength features (Bell and Watts, 1986). However, there are still some important

gaps in this data set (Fig. 2.2a) and therefore, we used satellite gravity data which have been proven to be quite accurate (Neumann et al., 1993; Marks, 1996; Sandwell and Smith, 1997).

Figure 2.2b is comparison between shipboard and satellite gravity data in the Ulleung Basin. It shows many spurious features that we described. However, in general, the overall trend is very much similar to satellite data. In our analysis, we used the satellite data due to two important reasons: (1) satellite data provide complete coverage over the sea and (2) our study focuses on long wavelength features reflecting the deep structure. Figure 2.3 shows the free-air gravity anomaly used for analysis. As expected, it matches well with the topography of the Ulleung Basin. The gravity anomaly within the Ulleung Basin varies from -20 to 20 mGal.

In the analysis of gravity anomalies to understand crustal structure, one of the most contentious issues is the precise determination of sediment thickness. As mentioned earlier, there have not been many studies aimed at resolving the deep structure except for a couple of cases. Hence, it is difficult to place too much confidence in areas not constrained by seismic observations.

Previous gravity investigation by Park et al. (2009) relied on the sediment thickness model compiled by the National Geophysical Data Center (NGDC) of NOAA (National Oceanic and Atmospheric Administration). This data set has a resolution of 5 x 5 arc min. In this study, we use the sediment-thickness information compiled by Lee et al. (2001), which is based largely on the interpretation of multi-channel seismic reflection profiles of KNOC and KIOST. The coverage of tracklines in Lee et al. (2001) is slightly better than that used by Park et al. (2009). Still, there are

substantial uncertainties, especially in the southern part where the sediment thickness is greater than 10 km. Figure 2.4 is the gridded basement map of the Ulleung Basin. With respect to a small basement high along WWS the basin can be roughly divided into north and south. We referred to them as north and south basins.

The residual gravity anomaly (RGA) was acquired by eliminating the gravitational effect of seafloor and sediment thickness from satellite-derived gravity data. We used 1.0, 2.3, 2.9 and 3.3 g/cm^3 as the density of water, sediments, crust and mantle, respectively. Gravitational effects by the undulation of the interfaces were calculation by Parker (1972) method.

An important cause of the resulting RGA is crustal thickness, assuming the density of mantle is uniform throughout the entire basin. We used Parker-Oldenburg iterative method (Oldenburg, 1974; Parker, 1972) from gravity anomaly to derive variation in the depth of Moho. Using this method, the crust-mantle interface iteratively in the Fourier domain based on the mean depth of the Moho and density values of the crust and mantle was calculated. As for the average Moho depth, 20 km was chosen. This value is roughly similar to previous seismic studies in the Ulleung Basin and is less than that determined by Cho et al. (2006) which showed that the depth of the Moho underneath Korean Peninsula is about 30 km.

2.4. Result

The RGA is shown in Figure 2.5. The RGA in the northern part of the Ulleung Basin is higher than those in the southern part. An abrupt change of the RGA is

observed in the western and southern boundaries of the basin, which is affected by surrounded continents such as SE Koran Peninsula and SW Japan Islands.

Figure 2.6 illustrates the variations in the Moho beneath the Ulleung Basin derived from the RGA. Instead of showing the entire region, we separate the areas where the thickness of sediment is constrained seismologically and the remaining areas by color shading the former whereas just plotting the contours for the latter. This ensures us from making errant interpretation in areas where there is almost no data.

The Moho depth varies from 16 to 22 km with high values along the outer rims of the basin and low values in the central part as anticipated. The letter H denotes the point where the depth of Moho is considered to be the highest, and the dashed line is the extrapolation of such low-value region in the WWS direction (Fig. 2.6). This line is located roughly between the seamounts to the north and basement median high to the south.

Figure 2.6b is cross sectional view along A-A', B-B', C-C' and D-D'. The variations in crustal thickness in the central part of the Ulleung Basin do not appear to be as great as previously portrayed. Although the lowest values are biased to the north, the overall undulation of Moho depth within the central part is not significant, only about 10% of the total thickness. In this particular case, the mean Moho depth of 15 km was used. However, assuming other values (greater and less than 5 km) did not alter this statement.

2.5. Thermal Consideration

Our model results show that the overall crustal thickness in the Ulleung Basin is almost uniform (Fig. 2.6b). However, we examine the gravitational effect by the other sources except for the undulation of the interfaces whether it could explain the variation of gravity anomaly in the Ulleung Basin. An important source of gravity anomaly is the variation in the density caused by differential cooling and heating. For instance, variations in the thickness of the crust during basin extension (often expressed in terms of stretching factor) can lead to difference in resulting thermal structure. Also, post-rift volcanism in certain area of the basin can also affect the mantle temperature in that part. However, it is difficult to estimate such effects without the detailed knowledge of basin evolution.

In this study, using simple analytic calculation, the effects of differential cooling and heating was estimated to check if they can also explain the variations in RGA. Within in the basin, the RGA varies by 80 mGal. In particular, two sets of cases were considered: one where the stretching factor was varied and the other where the mantle potential temperature was varied. Figure 2.7 shows the model that we used. The lithospheric thickness of 100 km undergoing stretching and cooling was considered. The stretching factor for 2 and 3 and the potential temperature for 1300 and 1400°C were considered. Half-space cooling model was used to calculate the geotherms after pure shear style opening occurred (McKenzie, 1978). The base temperature of the lithosphere was set at 1000°C.

Figure 2.8 represents the gravity anomaly for different mantle temperatures and stretching factors at the time of basin formation 25 Ma. It is important to note that

in our model we only consider for thermal conduction in the vertical direction. So the values represent in this model can be regard as the maximum possible estimate. According to Figure 2.8, the different values of stretching factor can produce large variation in gravity anomaly in the Ulleung Basin. In contrast, the increase of mantle potential temperature could not have a large influence on the variation of gravity anomaly (Fig. 2.8a).

2.6. Discussion

There are large gaps in the observations regarding the deep structure of Ulleung Basin. For instance, we have very little constraint on the Moho depth seismologically, and the thickness of sediment is not well defined except along several tracklines, especially in the southern part where sediment is the thickest. Therefore, conducting gravity analysis based on unconstrained interpolated information can be misleading. An important difference between an earlier examination of Ulleung Basin from the analysis of gravity (Park et al., 2009) and this study is that we made careful notice to interpret the data only in the regions where there are data. This approach not only allows us to provide a more reliable overall picture but also a more precise analysis and interpretations on sections where there are constraints.

The primary feature of the Ulleung Basin is that the central part is characterized by thin crust (16 km depth on average) whereas the outer edges have thick crust (24 km depth on average) (Fig. 2.6). A large difference between the center of the basin and the outer edges is not unexpected and can be seen in many other basins (Bassi et al., 1993; Keen and Dehler, 1997). In our view, the most important finding is

that within the central part of the basin, there is no evidence for large change in crustal thickness as previously shown. This is consistent with ocean bottom seismometers (OBS) studies conducted so far (Kim et al., 1998; 2003; Lee et al., 1999). They do not report significant change in Moho depth in the central part of the basin. Recently, seismic surveys using OBS and multi-channel streamer were carried out in the Yamato Basin near the Ulleung Basin and resulted in that there is also no large difference in the crustal thickness similar to that of the Ulleung Basin (Sato et al., 2015).

It is important to note that gravity can only represent the difference as opposed to the absolute value. In our study, we chose 20 km as the mean value in the inversion because that makes the thickness of the outer edges on the Korean Peninsula side more or less with the Moho depth of 30 km determined by seismological studies on land (Chang and Baag, 2005; Cho et al., 2006). Also, the average crustal thickness of 12 km in the center of the basin is roughly consistent with stretching factor of 2 - 3 based on 2D isostatic flexural investigation along deep seismic lines by Lee et al. (2003).

In general, the distribution of gravity anomaly in the Ulleung Basin appears to be consistent with pull-apart model suggested by Yoon et al. (2014). According to this model, Ulleung Basin formed as an extensional basin driven by a pair of right-lateral strike-slip faults. The exact location and definition of the driving faults are somewhat unclear at this stage, especially on the eastern side where the fault system counterpart to those on the eastern margin of Korea should be located between the Ulleung and Yamato basins. However, the observation that the line of high RGA is more or less consistent with the location and orientation of the axis of the pull-apart basin suggests that the opening indeed may have occurred in such a manner.

Another important feature in the resulting RGA map is that the location of high values. As mentioned earlier, we only need about 10 % variations in crustal thickness, which is not very much but still meaningful. According to Figure 2.6, the line of high values is biased to the north not very far from the volcanic islands (Ulleung and Dok islands) and post-rift volcanic edifices are found as opposed to the center of the Ulleung Basin. Furthermore, the highest Moho depth is located at the northeastern tip (marked as 'H' in Fig. 2.6). Such pattern may have significant implications for the nature of crustal thinning in the Ulleung Basin.

It appears that there was a slight crustal thinning associated with extension in the Ulleung Basin at the time of formation. However, our gravity analysis shows that the crustal thickness is almost uniformly in the Ulleung Basin, which may be a consequence of the post-rift underplating by the emplacement of magmatic body (Fig. 2.10). The decompressional melting by extensional forces generates the amount of melt and then it emplaced within the lower crust, which may result in decreasing the variation of the crustal thickness in the Ulleung Basin. However, our argument is speculative, and in order to validate it, detailed seismological investigation is needed.

In the western part of the Ulleung Basin, large intrusive magmatic body is occurred at 130.3°E and 37°N (Fig. 2.6) (Kim et al., submitted). Although it is not a very large feature, its proximity to the gravity measurements (at the sea surface) makes it important as source of additional gravity anomaly. In this study, we used simple model to understand the effects of such body in the gravity anomaly. The size and depth of the intrusive volcano are approximately calculated from the seismic reflection profile in Kim et al. (submitted). As shown in Figure 2.9, calculated gravity anomaly from simple model varies from 5 to 15 mGal using the densities of intrusive volcano of

2.4, 2.5 and 2.6 g/cm^3. Also, we could not exclude the possibility that more intrusive magmatic bodies in the sediment based on the distribution of the volcanic edifices in the northern part of the basin (Kim et al., 2011a). Therefore, although the gravity anomaly by the intrusive magmatic body is not large, we could not ignore the gravitational effect by the intrusive volcano.

The northern extent of high RGA in the northeast corner of the Ulleung Basin which we interpret as a region of opening axis is uncertain. Although in our map, the region stops just before the volcanic islands (Ulleung and Dok islands), such feature needs to be investigated further because the internal density structure of young volcanic islands can be different from the basin center composed of extended crust. Unfortunately, we have little understanding and constraint on this issue. However, if such region does extend further to the north and overlaps with major volcanic features, it will tie in much better with our argument of thermal erosion and the possible source of post-rift volcanism. However, at the moment, there is significant distance (45 to 60 km) between the region of high RGA and post-rift manifestations of magmatism, and it is uncertain if magma can be supply over such a distance, although linear distribution of volcanic edifices suggests that faulting played an important role.

The distribution of RGA (Fig. 2.6) and the general morphology of the crustal basement (Fig. 2.4) allow us to speculate on the origin of so-called median high located south of RGA highs. In this study, we interpret the median high as a bulge caused by sediment loading in the south (Fig. 2.10). Such kind of bulge resulting from loading on the other end of the basin is commonly found in many tectonic settings (DeCelles and Giles, 1996). Unfortunately, we have estimates on sediment thickness only on the Korean side of the sea. However, it is very likely that thick sediment

extends in the Japanese side as well. For now, this area on Japanese side is shown as blank in the maps.

In this study, we also consider the different conditions of thermal cooling using simple semi-analytical modeling. In particular, variation in mantle potential temperature and stretching factor (degree of extension) were considered. Because we have so little knowledge on the thickness of crust from direct seismological observations, it is hard to access how much the variations of these parameters would have affected the gravity anomaly. In our modeling, we only consider vertical heat conduction. If one considered lateral diffusion of heat, the effects of thermal anomalies would be less. However, it is important to note that the lateral variations in stretching factor can explain the variation in RGA within in Ulleung Basin but the lateral variation of potential temperature does not have largely effect on the variation in RGA (Fig. 2.9). The fact that even such small difference can account for the gravity anomaly illustrates that precise mapping of the Moho using seismic method is important in interpreting the gravity structure.

2.7. Conclusions

We investigate the gravity data in the Ulleung Basin using more extensive data sets than before, particularly focusing on the thickness of the crust. We also interpret the data only in the regions where there are data in order to provide a more reliable and precise analysis. Our investigations can be summarized as follows.

1. The high gravity anomaly is distributed in the central Ulleung Basin compared to the

outer edges, caused by the difference of the crustal thickness between the center and margins of the basin. However, the variation in crustal thickness is only about 10% within the central part of the basin, consistent with OBS studies.

2. The distribution of high RGA is consistent with the location and orientation of the axis of the pull-apart basin, which suggests that the basin opening may have occurred in such a manner.

3. The high RGA is biased to the north of the basin, not far from the volcanic edifices. Such post-rift volcanism in the north may cause magmatic underplating which results in decreasing the variation of the crustal thickness within the basin. The basement median high located south of RGA highs is interpreted as a bulge caused by sediment loading in the south.

4. A simple time-dependent thermal model for different stretching parameters and mantle potential temperature was constructed to examine the effect of temperature on the gravity anomaly. As a result, the lateral variations in stretching factor can explain the variation in RGA within in Ulleung Basin but the lateral variation of potential temperature does not have largely effect on the variation in RGA.

5. Our calculations show that a small change in tectonic parameters can lead to similar effect on gravity anomaly in the Ulleung Basin but the high RGA in the north may be affected by the post-rift volcanism. To resolve the ambiguity in the crustal structure, a more detailed and extensive deep seismic investigation is needed in the Ulleung Basin.

2.8. References

Barker, P.F., 1995. Tectonic framework of the east Scotia Sea. In: Taylor, B. (Ed.), Backarc Basins: Tectonics and Magmatism. Springer, US, pp. 281-314.

Bassi, G., Keen, C.E., Potter, P., 1993. Contrasting styles of rifting: models and examples from the eastern Canadian margin. Tectonics 12 (3), 639-655.

Bell, R.E., Watts, A.B., 1986. Evaluation of the BGM-3 sea gravity meter system onboard R/V Conrad. Geophysics 51 (7), 1480–1493.

Chang, S.J., Baag, C.E., 2005. Crustal structure in southern Korea from joint analysis of teleseismic receiver functions and surface-wave dispersion. Bull. Seismol. Soc. Am. 95 (4), 1516-1534.

Cho, H.M., Baag, C.E., Lee, J.M., Moon, W.M., Jung, H., Kim, K.Y., Asudeh, I., 2006. Crustal velocity structure across the southern Korean Peninsula from seismic refraction survey. Geophys. Res. Lett. 33, L06307.

Chough, S.K., Lee, H.J., Yoon, S.H., 2000. Marine geology of Korean seas. Elsevier, Amsterdam.

Christeson, G.L., Karson, J.A., McIntosh, K.D., 2010. Mapping of seismic layer 2A/2B boundary above the sheeted dike unit at intermediate spreading crust exposed near the Blanco Transform. Geochem. Geophys. Geosyst. 11 (3), Q03015.

Christeson, G.L., McIntosh, K.D., Karson, J.A., 2007. Inconsistent correlation of seismic layer 2a and lava layer thickness in oceanic crust. Nature 445 (7126), 418-421.

DeCelles, P.G., Giles, K.A., 1996. Foreland basin systems. Basin Res. 8 (2), 105-123.

Honza, E., Yuasa, M., Ishibashi, K., 1978. Geological investigations in the northern margin of the Okinawa Trough and the western margin of the Japan Sea. Geol. Surv. Japan Cruise Rp. 10, 39–42.

Horozal, S., Lee, G.H., Bo, Y.Y., Yoo, D.G., Park, K.P., Lee, H.Y., Kim, W., Kim, H.J., Lee, K., 2009. Seismic indicators of gas hydrate and associated gas in the Ulleung Basin, East Sea (Japan Sea) and implications of heat flows derived from depths of the bottom-simulating reflector. Mar. Geol. 258 (1), 126-138.

Jolivet, L., Tamaki, K., 1992. Neogene kinematics in the Japan Sea region and volcanic activity of the northeast Japan arc. In: Tamaki, K., Suyehiro, J., Allan, M., McWilliams et al. (Eds.), Proc. ODP, Sci Results 127/128 (Part 2). Ocean Drilling Program, College Station, TX, pp. 1311–1331.

Jolivet, L., Tamaki, K., Fournier, M., 1994. Japan Sea, opening history and mechanism: A synthesis. J. Geophys. Res. Solid Earth (1978–2012) 99 (B11), 22237-22259.

Keen, C.E., Dehler, S.A., 1997. Extensional styles and gravity anomalies at rifted continental margins: some North Atlantic examples. Tectonics 16 (5), 744-754.

Kim, G.B., Lee, S.M., Yoon, S.H., submitted, A new insight into asymmetric development of back-arc basin and tecto-magmatic evidences from the Ulleung Basin, East Sea (Japan Sea).

Kim, G.B., Yoon, S.H., Chough, S.K., Kwon, Y.K., Ryu, B.J., 2011a. Seismic reflection study of acoustic basement in the South Korea Plateau, the Ulleung Interplain Gap, and the northern Ulleung Basin: volcano-tectonic implications for Tertiary back-arc evolution in the southern East Sea. Tectonophysics 504 (1), 43-56.

Kim, G.Y., Yi, B.Y., Yoo, D.G., Ryu, B.J., Riedel, M., 2011b. Evidence of gas hydrate from downhole logging data in the Ulleung Basin, East Sea. Mar. Pet. Geol. 28 (10), 1979-1985.

Kim, H.J., Han, S.J., Lee, G.H., Huh, S., 1998. Seismic study of the Ulleung Basin crust and its implications for the opening of the East Sea (Japan Sea). Mar. Geophys. Res. 20 (3), 219-237.

Kim, H.J., Jou, H.T., Cho, H.M., Bijwaard, H., Sato, T., Hong, J.K., Yoo, H.S., Baag,

C.E., 2003. Crustal structure of the continental margin of Korea in the East Sea (Japan Sea): evidence for rifting affected by the hotter than normal mantle. Tectonophysics 364, 25–42.

Kinsman, D.J.J., 1975. Rift valley basins and sedimentary history of trailing continental margins. In: Fischer, A.G., Judson, S. (Eds.), Petroleum and Global Tectonics. Princeton University Press, pp. 83-126.

Lee, G.H., Kim, H.J., Han, S.J., Kim, D.C., 2001. Seismic stratigraphy of the deep Ulleung Basin in the East Sea (Japan Sea) back-arc basin. Mar. Pet. Geol. 18 (5), 615-634.

Lee, G.H., Kim, H.J., Suh, M.C., Hong, J.K., 1999. Crustal structure, volcanism, and opening mode of the Ulleung Basin, East Sea (Sea of Japan). Tectonophysics 308 (4), 503-525.

Lee, S.M., Kim, J.W., Baag, C.E., 2003. 2-D flexural analysis of the Ulleung back-arc basin, East Sea (Sea of Japan). Terr. Atmos. Ocean. Sci. 14 (4), 431-444.

Leeds, A.R., Knopoff, L., Kausel, E.G., 1974. Variations of upper mantle structure under the Pacific Ocean. Science. 186 (4159), 141-143.

Ludwig, W.J., Murauchi, S., Houtz, R.E., 1975. Sediments and structure of the Japan Sea. Geol. Soc. Am. Bull. 86 (5), 651-664.

Marks, K.M., 1996. Resolution of the Scripps/NOAA marine gravity field from satellite

altimetry. Geophys. Res. Lett. 23 (16), 2069–2072.

McKenzie, D., 1978. Some remarks on the development of sedimentary basins. Earth Planet. Sci. Lett. 40 (1), 25-32.

Neumann, G.A., Forsyth, D.W., Sandwell, D., 1993. Comparison of Marine Gravity From Shipboard and High-Density Satellite Altimetry Along the Mid-Atlantic Ridge, 30.5 -35.5 S. Geophys. Res. Lett. 20 (15), 1639-1642.

Okino, K., Kasuga, S., Ohara, Y., 1998. A new scenario of the Parece Vela Basin genesis. Mar. Geophys. Res. 20 (1), 21-40.

Oldenburg, D.W., 1974. The inversion and interpretation of gravity anomalies. Geophysics 39 (4), 526-536.

Park, C.H., Kim, J.W., Isezaki, N., Roman, D.R., von Frese, R.R., 2006. Crustal analysis of the Ulleung Basin in the East Sea (Japan Sea) from enhanced gravity mapping. Mar. Geophys. Res. 27 (4), 253-266.

Park, G.S., Park, J.S., Kwon, B.D., Kim, C.H., Park, C.H., 2009. Tectonic structure modeling around the Ulleung Basin and Dokdo using potential data. J. Korean Earth Sci. Soc. 30 (2), 165-175.

Parker, R.L., 1972. The rapid calculation of potential anomalies. Geophys. J. R. Astron. Soc. 31 (4), 447-455.

Sandwell, D.T., Smith, W.H., 1997. Marine gravity anomaly from Geosat and ERS 1 satellite altimetry. J. Geophys. Res. 102, 10039-10054.

Sato, T., No, T., Miura, S., Kodaira, S., Ishiyama, T., Sato, H., 2015. Relation between the crustal structure type and the distribution of the crustal deformation in the Japan Sea back-arc basins and its margins. Abstract T31B-2876 presented at 2015 AGU Fall meeting, AGU, San Francisco, USA.

Sato, T., Sato, T., Shinohara, M., Hino, R., Nishino, M., Kanazawa, T., 2006. P-wave velocity structure of the margin of the southeastern Tsushima Basin in the Japan Sea using ocean bottom seismometers and airguns. Tectonophysics 412 (3), 159-171.

Sdrolias, M., Roest, W.R., Müller, R.D., 2004. An expression of Philippine Sea plate rotation: the Parece Vela and Shikoku basins. Tectonophysics 394 (1), 69-86.

Sohn, Y.K., 1995. Geology of Tok Island, Korea: eruptive and depositional processes of a shoaling to emergent island volcano. Bull. Volcanol. 56 (8), 660-674.

Sohn, Y.K., Park, K.H., 1994. Geology and Evolution of Tok Island, Korea. J. Geol. Soc. Korea. 30 (3), 242-261.

Tamaki, K., Suyehiro K., Allan J., Ingle J.C., Jr., Pisciotto, K.A., 1992. Tectonic synthesis and implications of Japan Sea ODP drilling. In: Tamaki, K., Suyehiro, J., Allan, M., McWilliams et al. (Eds.), Proc. ODP, Sci Results 127/128 (Part 2). Ocean Drilling Program, College Station, TX, pp. 1333–1348.

Taylor, B., Zellmer, K., Martinez, F., Goodliffe, A., 1996. Sea-floor spreading in the Lau back-arc basin. Earth Planet. Sci. Lett. 144 (1), 35-40.

Veevers, J.J., 1981. Morphotectonics of rifted continental margins in embryo (East Africa), youth (Africa-Arabia), and maturity (Australia). J. Geol. 57-82.

Yoon, S.H., Sohn, Y.K., Chough, S.K., 2014. Tectonic, sedimentary, and volcanic evolution of a back-arc basin in the East Sea (Sea of Japan). Mar. Geol. 352, 70-88.

2.9. Figures

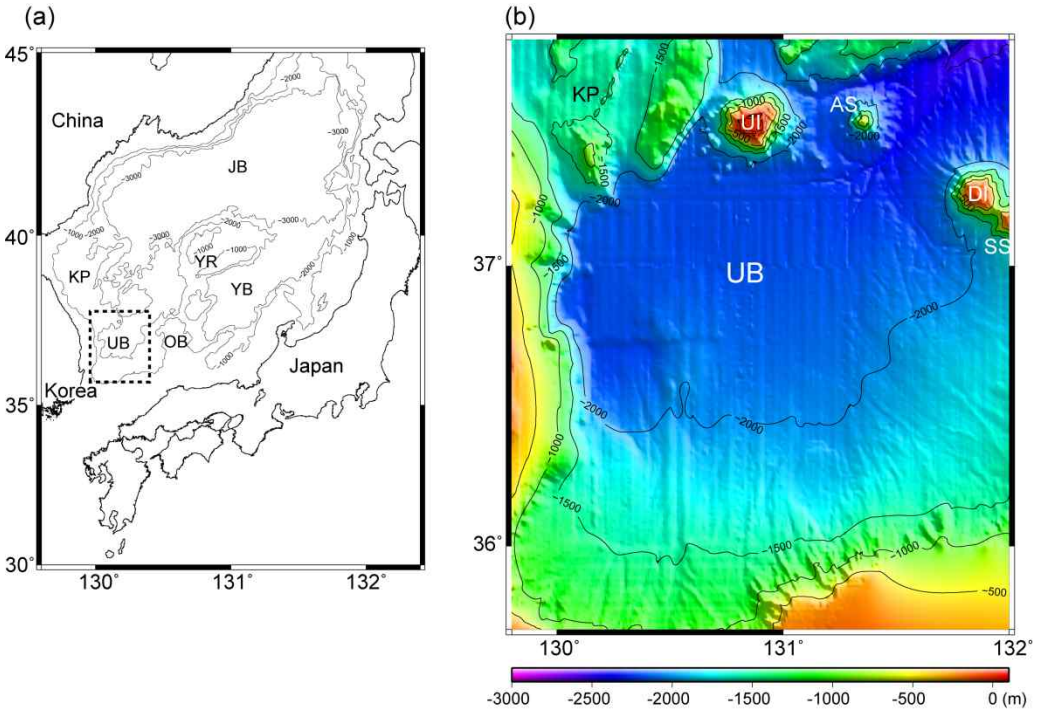

Figure 2.1 (a) Physiographic map of the East Sea/Sea of Japan. Dotted box locates the study area. JB, YB and UB: Japan, Yamato and Ulleung basins, KP: Korea Plateau, YR: Yamato Ridge, OB: Oki Bank. (b) Bathymetric map of the Ulleung Basin and contour interval is 500 m. UI: Ulleung Island, AS: Anyongbok Seamount, DI: Dok Island, SS: Simheungtaek Seamount

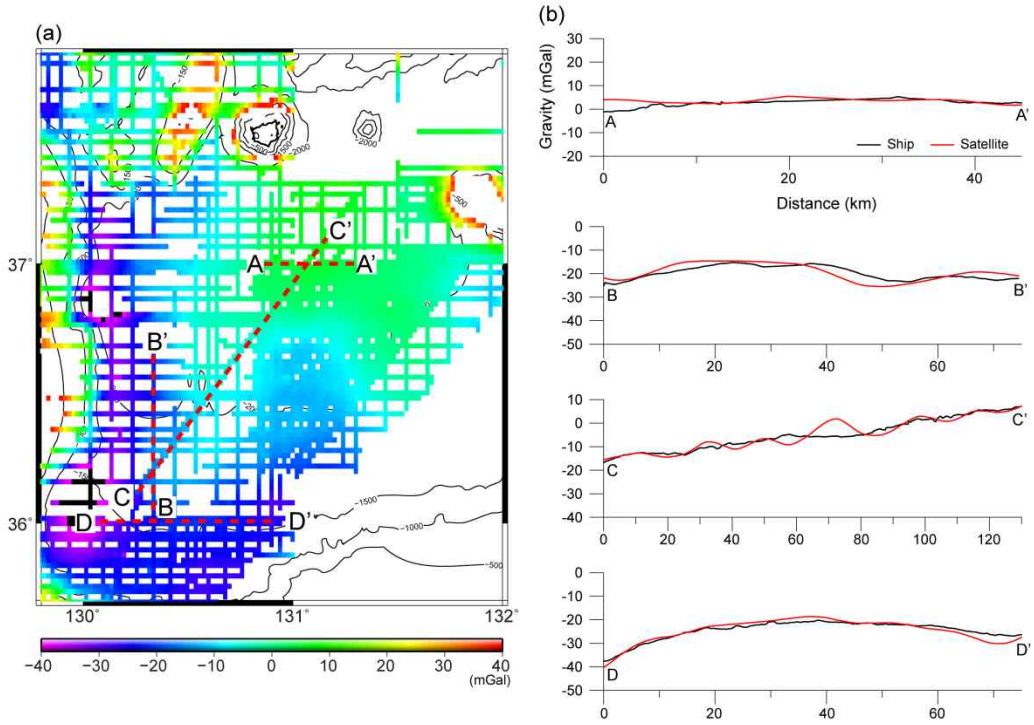

Figure 2.2 (a) Color shaded-relief free-air gravity anomaly map superimposed onto bathymetry. The free-air gravity was measured by R/V Tamhae II from 1997 to 2014. Contour lines of bathymetry are at 500 m depth interval. The red dotted lines locate the gravity comparison in (b). (b) Comparison between shipboard gravity data (black) and satellite-derived gravity data (red). The satellite gravity data is derived from satellite altimeters (Sandwell and Smith, 1997).

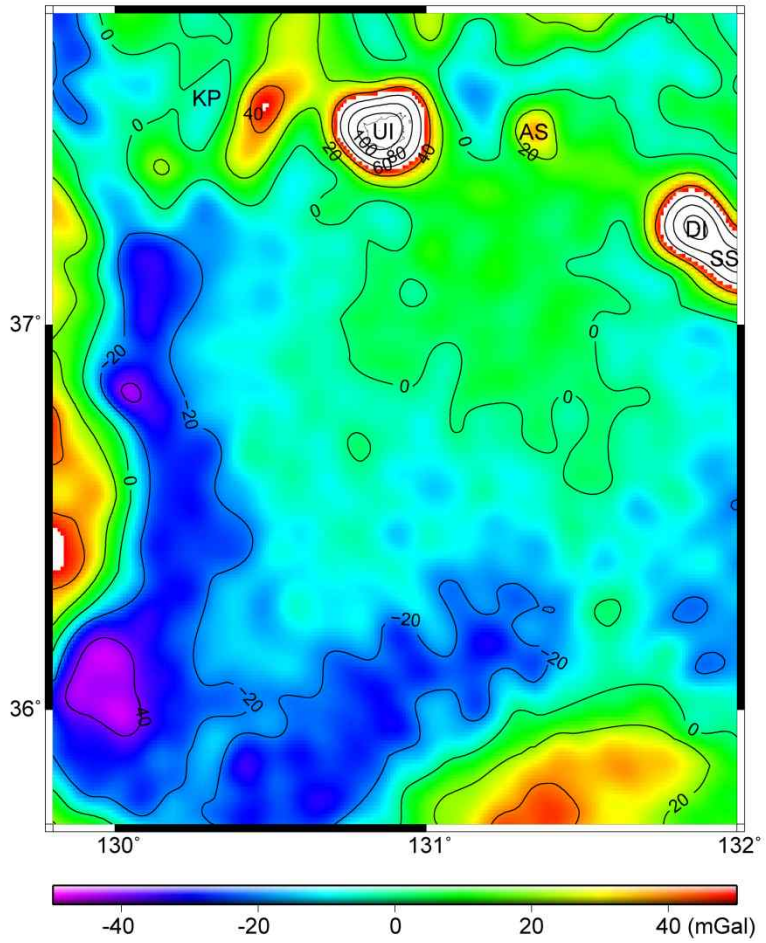

Figure 2.3 Free-air gravity anomaly map derived from the satellite altimeters. Contour interval is 20 mGal and abbreviations are same in Fig. 2.1.

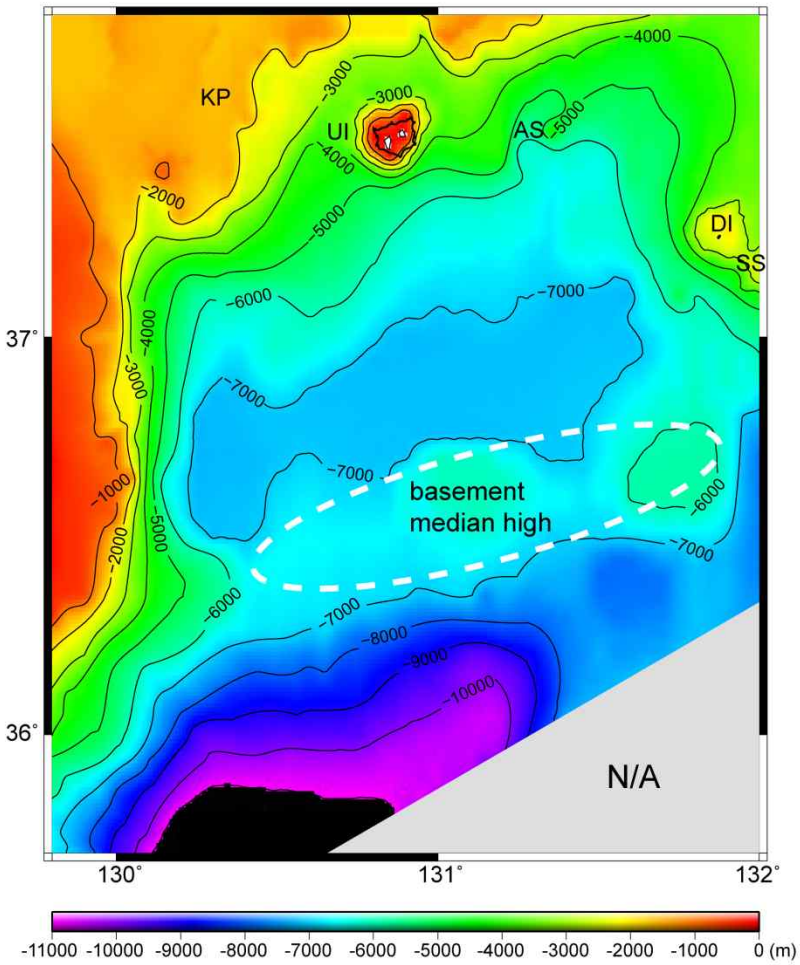

Figure 2.4 Basement topography map. Contour interval is 1000 m and gray shading at right corner denotes the region where the data of sediment thickness is not available. The white dotted line encloses the region of basement median high and abbreviations are same in Fig. 2.1.

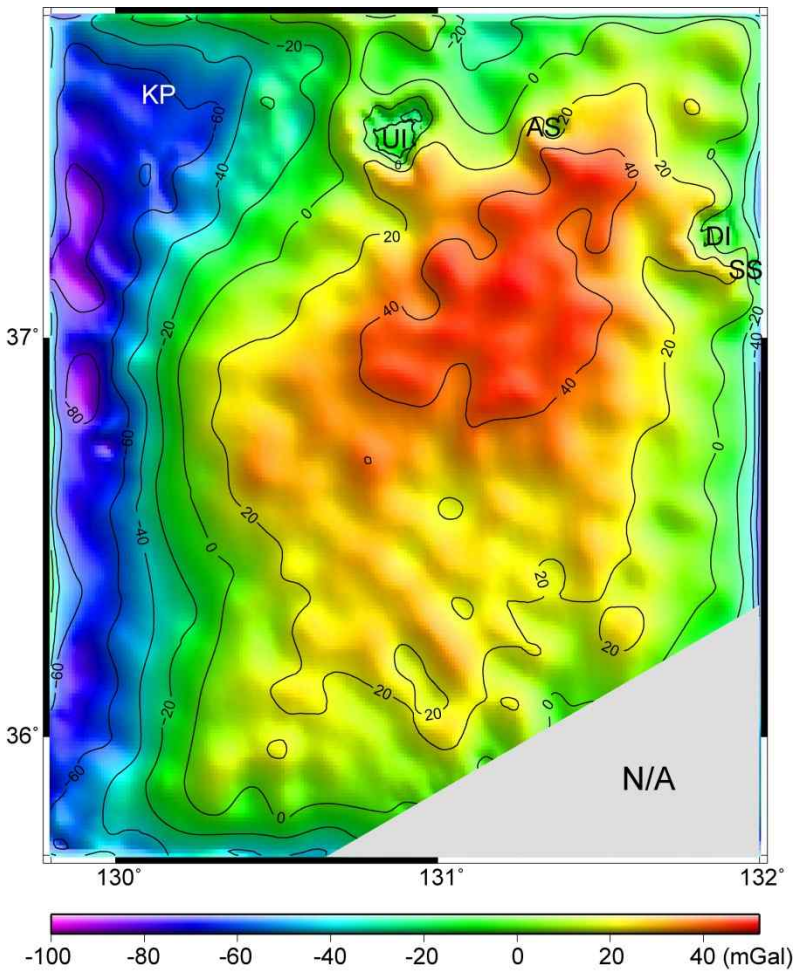

Figure 2.5 Residual gravity anomaly (RGA) map eliminated the gravitational effect of the seafloor and sedimentary basement from the free-air anomaly. Contour interval is 20 mGal. Abbreviations are same in Fig. 2.1 and gray shading is the same as shown in Fig. 2.4.

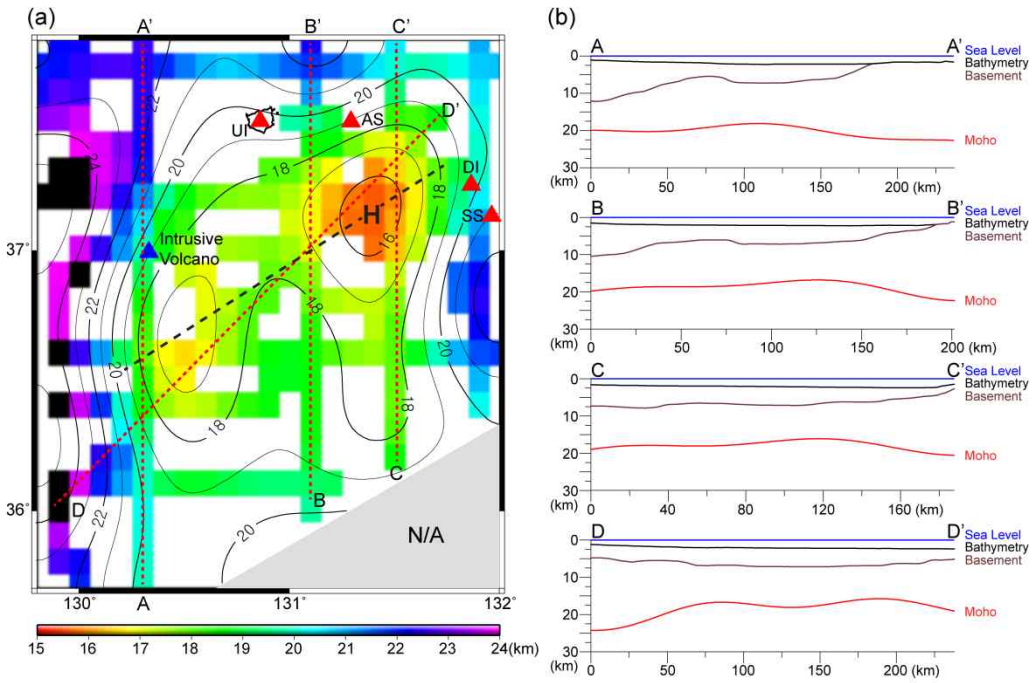

Figure 2.6 (a) Shaded-relief map of the Moho discontinuity derived from residual gravity anomaly (RGA). Color shaded is the area where the data of sediment thickness is reliable in the Ulleung Basin. The contour interval is 1 km. 'H' indicates the region showing the highest Moho topography and the black dashed line is the extrapolation of high-value of the Moho depth. The red dotted lines denote the location of cross sections in (b). Red triangles is volcanic edifices erupted during the Quaternary period and blue triangle indicates the location of intrusive magmatic body. Abbreviations are same in Fig. 2.1 and gray shading is the same as shown in Fig. 2.4. (b) Cross sectional views showing the boundaries of the water, sediment, crust and mantle across the A-A', B-B', C-C' and D-D' lines in (a).

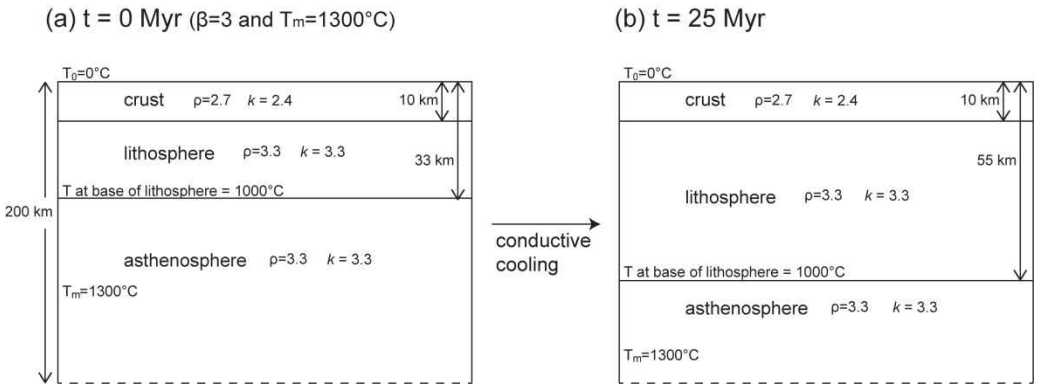

Figure 2.7 Schematic diagrams indicating the thermal model for the Ulleung Basin assuming mantle potential temperature of 1300 °C and stretching factor of 3 (Crustal and lithospheric thickness decrease from 30 to 10 and 100 to 33 km, respectively.). The half-space cooling model was used to calculate the geotherms and pure shear opening of McKenzie (1978) is applied. (a) At time = 0 Myr, extension of the basin occurs instantaneously and causes upwelling of the asthenosphere. The lithosphere cools down by thermal conduction and thickens with age. The temperature of base of the lithosphere is assumed as 1000°C (Leeds et al., 1974). (b) At time = 25 Myr after instantaneous thinning by lateral stretching for β=3, the thickness of lithosphere goes down at about 55 km by thermally conductive cooling. The units of density (ρ) and thermal conductivity (k) are g/cm^3 and W/m/K, respectively.

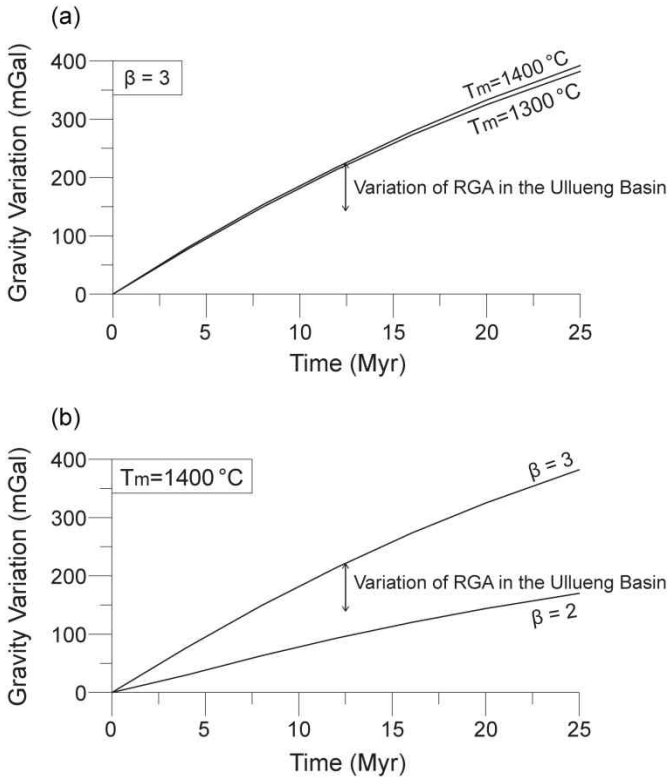

Figure 2.8 Variation of gravity anomaly by conductive cooling during 25 Myr after instantaneous thinning. The stretching factor (β) for 2 and 3 and the potential temperature (Tm) for 1300 and 1400°C were used in our model (described in Fig. 2.7). (a) Fixed that stretching factor (β) is 3, comparison of gravity anomaly variation calculated using the mantle potential temperature (Tm) for 1300 and 1400°C. (b) Fixed that mantle potential temperature (Tm) is 1400°C, comparison of gravity anomaly variation calculated using the stretching factor (β) for 2 and 3. Double-headed arrow denotes the amount of the variation of the residual gravity anomaly (RGA) which is about 80 mGal in the Ulleung Basin (Fig. 2.5).

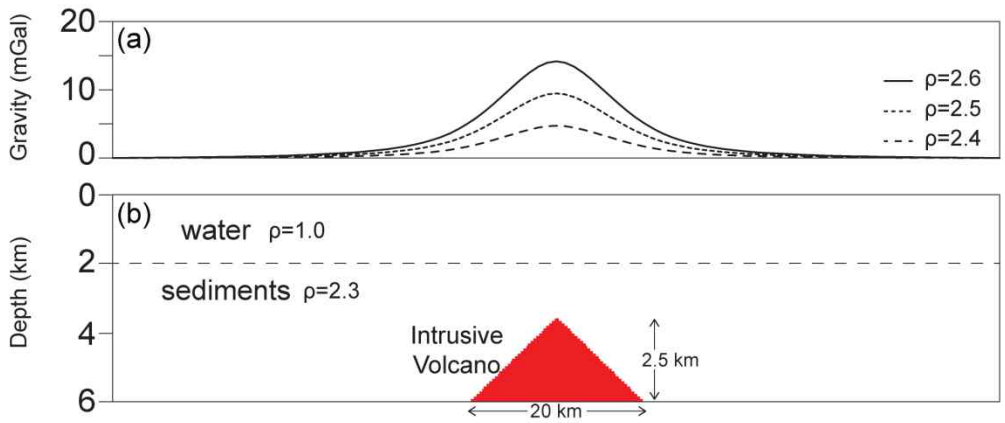

Figure 2.9 Simple diagram showing the gravity anomaly caused by intrusive volcano. (a) Gravity anomaly caused by 2.4 (dashed), 2.5 (dotted) and 2.6 g/cm^3 (solid) of intrusive volcano within the sediment described as red triangle in (b). (b) Profile of intrusive magmatic body including density values of water (1.0 g/cm^3) and sediment (2.3 g/cm^3). The width and height of the intrusive volcano are modified from Kim et al. (submitted) and its location is described in Fig. 2.6 (blue triangle).

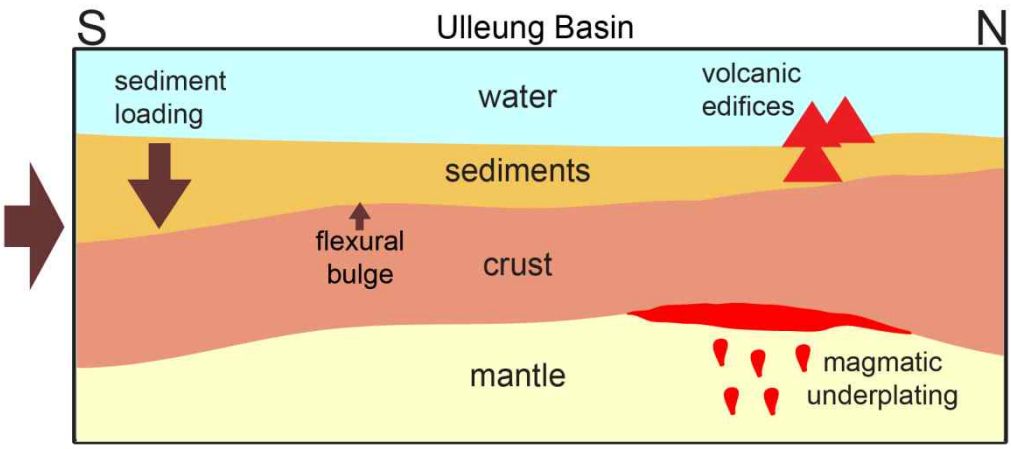

Figure 2.10 Model diagram illustrating the flexural bulge by sediment loading to the south and magmatic underplaing by volcanic edifices to the north of the Ulleung Basin.

요약 (국문초록)

위 학위 논문에서는 동해 울릉분지의 지구조적인 진화와 섭입대에서의 해양지각의 용융이 아다카이트와 보니나이트를 어떻게 생성하는가에 관한 연구를 다룬다. 본문에서는 크게 두 개의 주제로 구성되어 연구를 정리하였다.

첫 번째 연구는 시간에 따른 섭입 슬랩의 나이와 섭입 속도가 섭입대에서의 아다카이트와 보니나이트의 생성을 설명할 수 있는가에 대한 연구이다. 이것을 보이기 위하여 각각의 섭입대에 맞는 이차원적인 수치 모델을 만들었고 이것을 각 섭입대에서의 지화학적 증거와 비교하였다. 결과는 몇몇의 섭입대에서는 모델 결과가 실제 지화학적 증거와 잘 일치하였지만 마리아나와 북동 일본 섭입대 등 몇몇 지역에서는 모델 결과가 잘 맞지 않는 것을 확인 할 수 있었다. 이러한 모델과 맞지 않는 섭입대에서는 섭입 슬랩의 나이와 섭입 속도 이외에도 다른 지구조적 운동, 특히 배호 분지의 생성, 뜨거운 맨틀의 유입, 리지 섭입 등이 섭입대에서의 해양 지각의 용융을 설명하는 데 있어서 필요함을 알 수 있었다.

두 번째 연구는 울릉분지에서의 중력 자료 분석과 그것이 울릉분지의 지각 구조를 어떻게 해석하는지에 관한 것이다. 중력 자료를 가지고 울릉분지의 지각 구조를 해석하기 위하여 다방면의 계산을 수행하였으며 분지에서의 온도가 중력에 어느 정도로 영향을 미칠 수 있는가에 대해 알아보기 위해 열적 모델을 만들었다. 중력 분석 결과로 보면, 울릉 분지는 모호면이 16에서 22 km 정도이며 울릉분지 내에서의 모호면의 차이는 전체의 10-20 % 정도에 지나지 않는다. 이러한 결과는 기존의 탐사 자료와도 일치하며 위 논문에서는 울릉분지의 지각 구조를 살펴보고 분지 확장 이후의 울릉분지의 현 모습을 만든 프로세스에 관하여도 다룬다.